



ARTICLE

Expression of mutant *Asxl1* perturbs hematopoiesis and promotes susceptibility to leukemic transformation

Reina Nagase^{1*}, Daichi Inoue^{1,2*}, Alessandro Pastore² , Takeshi Fujino¹, Hsin-An Hou³, Norimasa Yamasaki⁴, Susumu Goyama¹, Makoto Saika¹, Akinori Kanai⁵, Yasuyuki Sera⁴, Sayuri Horikawa¹, Yasunori Ota⁶, Shuhei Asada¹, Yasutaka Hayashi¹, Kimihito Cojin Kawabata¹, Reina Takeda¹, Hwei-Fang Tien³, Hiroaki Honda^{4,7}, Omar Abdel-Wahab^{2**}, and Toshio Kitamura^{1**} 

Additional sex combs like 1 (ASXL1) is frequently mutated in myeloid malignancies and clonal hematopoiesis of indeterminate potential (CHIP). Although loss of ASXL1 promotes hematopoietic transformation, there is growing evidence that ASXL1 mutations might confer an alteration of function. In this study, we identify that physiological expression of a C-terminal truncated *Asxl1* mutant in vivo using conditional knock-in (KI) results in myeloid skewing, age-dependent anemia, thrombocytosis, and morphological dysplasia. Although expression of mutant *Asxl1* altered the functions of hematopoietic stem cells (HSCs), it maintained their survival in competitive transplantation assays and increased susceptibility to leukemic transformation by co-occurring *RUNX1* mutation or viral insertional mutagenesis. KI mice displayed substantial reductions in H3K4me3 and H2AK119Ub without significant reductions in H3K27me3, distinct from the effects of *Asxl1* loss. Chromatin immunoprecipitation followed by next-generation sequencing analysis demonstrated opposing effects of wild-type and mutant *Asxl1* on H3K4me3. These findings reveal that *ASXL1* mutations confer HSCs with an altered epigenome and increase susceptibility for leukemic transformation, presenting a novel model for CHIP.

Introduction

Additional sex combs like 1 (ASXL1) is frequently mutated in patients with all forms of myeloid malignancies, including myelodysplastic syndromes (MDS), chronic myelomonocytic leukemia, myeloproliferative neoplasms, and acute myeloid leukemia (AML) with MDS-related changes. In each of these diseases, mutations in *ASXL1* are consistently associated with poor prognosis and advanced age (Bejar et al., 2011; Thol et al., 2011; Haferlach et al., 2014).

Mutations in *ASXL1* most commonly occur in the last exon as frameshift and nonsense mutations before the C-terminal plant homeofinger domain (Bejar et al., 2011; Thol et al., 2011; Haferlach et al., 2014). In addition, similar *ASXL1* mutations are found in clonal hematopoiesis of indeterminate potential (CHIP; Genovese et al., 2014; Jaiswal et al., 2014; Xie et al., 2014), a condition associated with an increased likelihood of progression to myeloid malignancies. Previous work from us and others identified that

Asxl1 loss in vivo results in progressive multilineage cytopenias and dysplasia with increased numbers of hematopoietic stem and progenitor cells (HSPCs) and impaired mature cell differentiation consistent with features of human MDS (Abdel-Wahab et al., 2013; Wang et al., 2014). At the same time, we previously reported that these same features are recapitulated by retroviral overexpression of mutant *ASXL1* cDNA, suggesting that mutant forms of *ASXL1* may inhibit the function of WT *ASXL1* (Inoue et al., 2013). Moreover, recent work has suggested that expression of *ASXL1* mutations may also confer a gain of function by promoting the enzymatic activity of BRCA1-associated protein 1 (BAP1), a deubiquitinase known to promote histone H2A lysine 119 (H2AK119) deubiquitination (Balasubramani et al., 2015).

The above findings raise the question of whether the recurrent *ASXL1* mutations result in a loss of protein or expression of a truncated form lacking the C-terminal plant homeofinger

¹Division of Cellular Therapy, The Institute of Medical Science, The University of Tokyo, Tokyo, Japan; ²Human Oncology and Pathogenesis Program, Memorial Sloan-Kettering Cancer Center, New York, NY; ³Division of Hematology, Department of Internal Medicine, National Taiwan University Hospital, Taipei, Taiwan; ⁴Department of Disease Model, Research Institute for Radiation Biology and Medicine, Hiroshima University, Hiroshima, Japan; ⁵Department of Molecular Oncology and Leukemia Program Project, Research Institute for Radiation Biology and Medicine, Hiroshima University, Hiroshima, Japan; ⁶Department of Pathology, Research Hospital, The Institute of Medical Science, The University of Tokyo, Tokyo, Japan; ⁷Field of Human Disease Models, Major in Advanced Life Sciences and Medicine, Tokyo Women's Medical University, Tokyo, Japan.

*R. Nagase and D. Inoue contributed equally to this paper; **O. Abdel-Wahab and T. Kitamura contributed equally to this paper; Correspondence to Toshio Kitamura: kitamura@ims.u-tokyo.ac.jp; Daichi Inoue: inoued@mskcc.org.

© 2018 Nagase et al. This article is distributed under the terms of an Attribution–Noncommercial–Share Alike–No Mirror Sites license for the first six months after the publication date (see <http://www.rupress.org/terms/>). After six months it is available under a Creative Commons License (Attribution–Noncommercial–Share Alike 4.0 International license, as described at <https://creativecommons.org/licenses/by-nc-sa/4.0/>).

domain. The fact that mutations in *ASXL1* occur in a hotspot region located in the last exon and predicted to result in mutant transcripts that escape nonsense-mediated mRNA decay supports the possibility that most *ASXL1* mutations may generate a stable truncated protein (Inoue et al., 2016). Consistent with this, truncated mutant forms of *ASXL1* have been detected in leukemic cells with homozygous *ASXL1* mutations using mTRAQ-based mass spectrometric analysis (Inoue et al., 2016). These data suggest that expression of mutant *ASXL1* may be a more appropriate model to study the effects of *ASXL1* mutations rather than models with deletion of *ASXL1*. However, our prior data regarding the effects of mutant *ASXL1* expression to date have used retroviral overexpression, a method susceptible to experimental artifacts from supraphysiologic expression of cDNA, retroviral integration leading to up-regulation of neighboring genes, and forced cell cycle progression of quiescent hematopoietic stem cells (HSCs) when exposed to a high concentration of cytokines before transplantation (Cook and Pardee, 2013).

To overcome these limitations and evaluate the effects of mutant *Asxl1* expression on disease development and progression, we generated conditional *Asxl1* mutant knock-in (*Asxl1*-MT KI) mice. Hematopoietic expression of mutant *Asxl1* in this manner perturbed hematopoiesis but was not sufficient to transform HSCs. At the same time, mutant *ASXL1* expression increased susceptibility of HSCs to transformation from additional mutations provided by insertional mutagenesis or expression of mutant *RUNX1* (*Runt-related transcription factor 1*) or the *MLL-AF9* fusion oncogene. In addition, we identified differences in the direct binding targets of WT *Asxl1* and mutant and their distinct effects on histone modifications. These data provide a faithful model to study *ASXL1* mutations in vivo and explain the enrichment of *ASXL1* mutations in CHIP and early forms of MDS.

Results

Generation of conditional *Asxl1*-MT KI mice

To generate *Asxl1*-MT KI mice, we mimicked the well-described human *ASXL1* mutation, p.E635RfsX15 (Thol et al., 2011; Chen et al., 2014; Paschka et al., 2015). To allow for conditional *ASXL1* mutant expression with epitope and fluorescent tagging, a floxed neomycin and stop cassette followed by an N-terminal 3xFLAG-tagged mouse *Asxl1* mutant (1–1,890) cDNA followed by internal ribosome entry site (IRES)/enhanced GFP (EGFP) were inserted into the *Gt(ROSA)26Sor* (*Rosa26*) locus by homologous recombination (Fig. 1 A). Correctly targeted embryonic stem cells (ESCs) identified using 3' genomic PCR (Fig. 1 B) and Southern blotting with 5' genomic probes (Fig. 1 C) were used to create chimeric mice that transmitted the mutated allele through the germline. Mice carrying the floxed allele (3xFLAG-*Asxl1* mutant flox/flox-IRES-EGFP) were crossed with Vav-Cre transgenic mice, in which Cre recombinase is activated exclusively in the hematopoietic lineage (de Boer et al., 2003). Vav-Cre *Asxl1* mutant heterozygous (fl/wt) and homozygous (fl/fl) mice were born at expected Mendelian ratios (unpublished data) with no apparent developmental abnormality. PCR and Western blot analysis demonstrated Cre recombination and the expression of the mutant proteins exclusively in hematopoietic tissues (Fig. 1, D and E) with *Asxl1*-MT KI

cells clearly identified by GFP positivity (Fig. 1 F). Finally, Sanger sequencing and quantitative RT-PCR of cDNA from hematopoietic tissues confirmed expression of mutant *Asxl1* expression at levels comparable to the WT alleles, and we demonstrated no effect of *Asxl1* mutant on WT expression by quantitative RT-PCR and Western blotting (Fig. 1, G–I).

Characterization of *Asxl1*-MT KI mice

Examination of peripheral blood (PB) parameters revealed no significant change in younger mice (24 wk old; not depicted) and a reduction in red blood cell (RBC) counts and increase in mean cellular volume (MCV) and platelets in KI mouse at 70 wk of age (Fig. 2 A). We also observed increased frequency of CD11b⁺ myeloid cells, in particular, neutrophils (CD11b⁺ Gr1⁺), but not monocytes (CD11b⁺ Gr1[−]), in the PB and bone marrow (BM) and an increased proportion of neutrophils and CD11b⁺ c-Kit⁺ immature myeloid cells in the BM (although the total white blood cell [WBC] count did not significantly increase; Fig. 2, A–C; and Fig. S1, A and B). To further characterize anemia in the KI mice, we examined committed erythroid precursor maturation in the BM based on CD71 and Ter119 expression, which subdivides cells into several stages of erythroblast maturation (Chen et al., 2009; Liu et al., 2013). This revealed a modest block in erythroid development, characterized by an accumulation of cells in stage I and II of erythroblast maturation in the BM of KI mice, similar to previous findings in *Asxl1* KO mice (Shi et al., 2016; Fig. 2 D). Consistent with the thrombocytosis seen in KI mice, a connection between *ASXL1* mutations and higher platelet counts was seen in a cohort of MDS-refractory anemia patients. In this cohort, platelet counts were significantly higher in patients with *ASXL1* mutations than in those WT for *ASXL1* (median, 135,000/ μ l; range, 34,000–607,000 vs. 68,500/ μ l; range, 3,000–442,000, $P = 0.0068$). Although no hepatosplenomegaly or hypercellularity in the BM was detected at any age (Fig. 2 E), increased red pulp along with decreased follicles in the spleen were identified, suggesting more activated extramedullary hematopoiesis in the KI mice (Fig. S1 C). Moreover, histological analysis revealed increased megakaryocytes in the BM as well as spleen in the old KI mice (70 wk old; Figs. 2 F and S1 D). Finally, dysplastic features in the BM, including nucleated erythroid precursors, abnormal nuclear maturation, hypersegmentation, and megaloblastic change of erythroid lineage in relatively minor population, were detected (Figs. 2 G and S1 E).

Impaired HSC function in *Asxl1*-MT KI mice

We next determined whether expression of *Asxl1* mutant altered HSPC frequency by multiparameter flow cytometry. Intriguingly, there was a profound decrease in the frequency of BM Lin[−]Scal[−]c-Kit⁺ (LSK) cells, CD150⁺CD48[−] long-term repopulating HSCs (LT-HSCs), and CD150[−]CD48⁺ multipotent progenitors (MPPs; Fig. 3, A and B). Of note, we observed the increase in the number of megakaryocyte/erythroid progenitors (MEPs; Lin[−]c-Kit⁺Scal[−]CD34[−]FcyR[−]) in KI group, whereas other myeloid progenitor populations were not affected (Fig. 3, A and C). In addition, increased MEPs of KI mice were found to differentiate toward megakaryocyte progenitors (MkPs; CD41^{high}CD71^{low}MEP) rather than erythrocyte progenitors (ErPs; CD41^{low}CD71^{high}MEP;

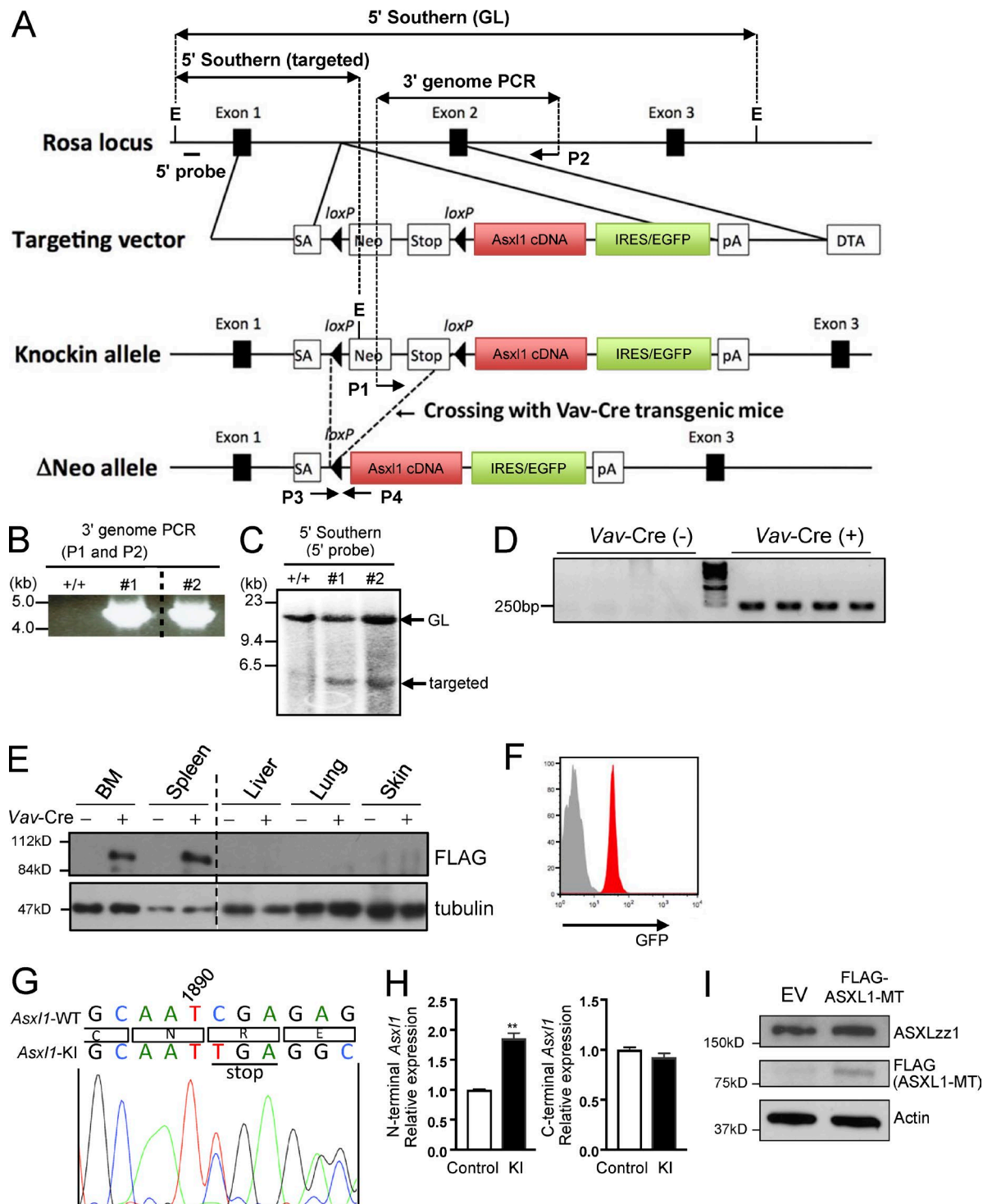


Figure 1. Generation of *Asxl1*-MT KI mice. (A) Schematic depiction of the targeted *Rosa* locus, targeting vector, *Asxl1*-MT KI allele, and neostop deleted allele. The coding sequence 1–1,890 followed by stop codon was used in *Asxl1* cDNA. DTA, diphtheria toxin A gene; EV, empty vector; GL, germline; SA, splicing acceptor. (B) Verification of correct homologous recombination. Using P1 and P2 primers in A, 3' genomic PCR was performed. (C) Verification of correct homologous recombination of *Asxl1*-MT KI allele by a 5' Southern blot using EcoRI-digested DNA and a 5' external probe. (D) Confirmation of recombination after crossing with Vav-Cre transgenic mice using P3 and P4 primers ($n = 4$ mice per group). (E) Expected expression of FLAG-tagged Asxl1 mutant proteins in the BM and spleen cells. (F) GFP positivity of BM sample in Vav-Cre-negative *Asxl1*-MT^{fl/fl} (gray) and Vav-Cre-positive *Asxl1*-MT^{fl/fl} (red) mice. (G) DNA sequences of PCR products derived from Vav-Cre-positive *Asxl1*-MT^{fl/fl} BM cells. Both WT and KI sequences with corresponding amino acids are shown on the top. (H) Relative expression of N-terminal Asxl1 and C-terminal Asxl1 mRNA were measured by quantitative RT-PCR. Vav-Cre-negative *Asxl1*-MT^{fl/fl} (control) and Vav-Cre-positive *Asxl1*-MT^{fl/fl} BM cells were used ($n = 3$ per group). (I) HEK293T cells were transiently transfected with empty vector and FLAG-ASXL1 mutant (1900–1922del; E635RfsX15). Expression of ASXL1, FLAG-ASXL1 mutant, and Actin was analyzed by Western blot. Data are presented as mean \pm SEM. **, $P < 0.01$ (Student's t test). Experimental data were verified in at least two independent experiments. We used Vav-Cre-negative *Asxl1*-MT^{fl/fl} mice as littermate controls.

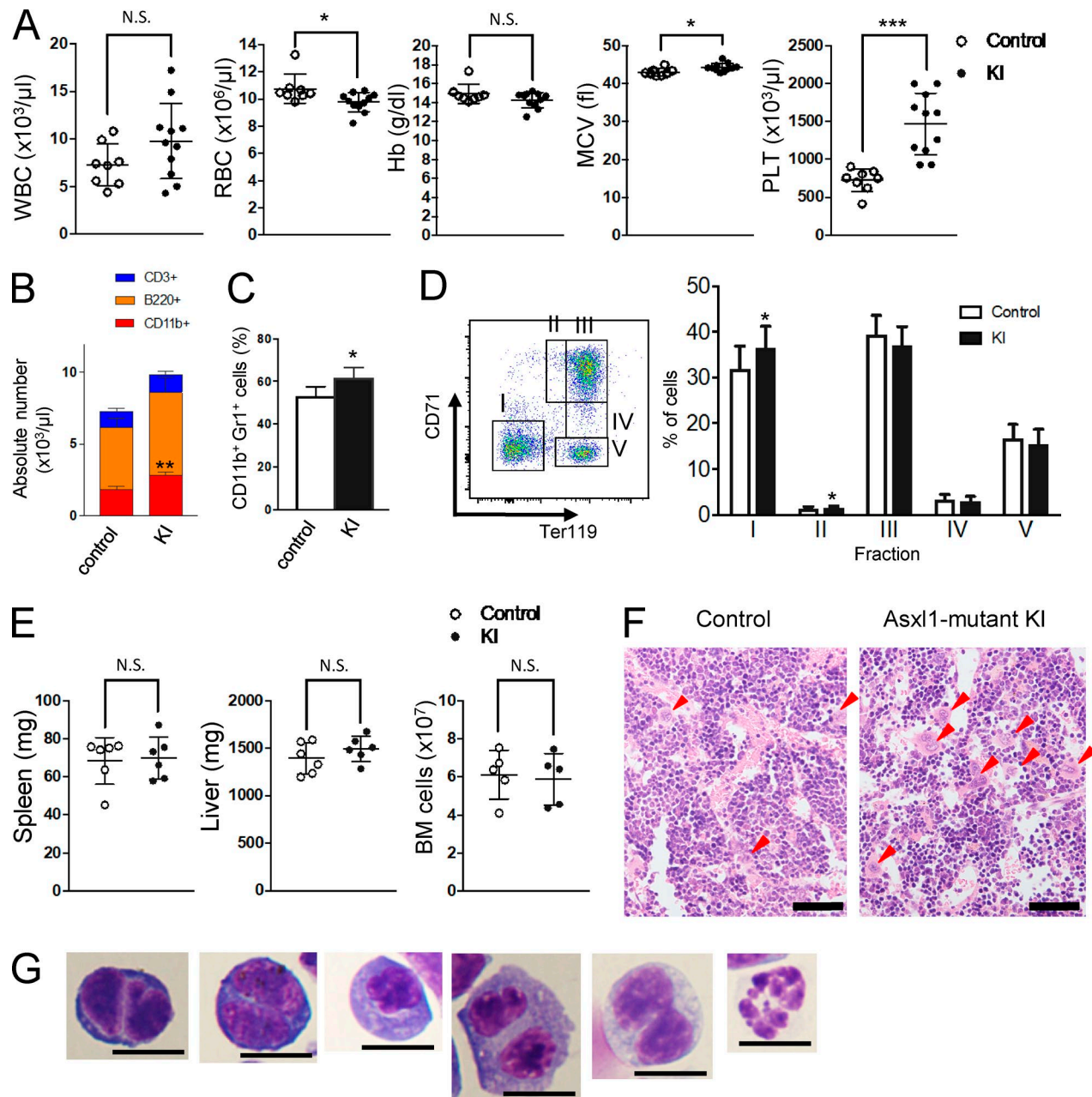


Figure 2. Phenotypic characterization of primary *Asxl1*-MT KI mice. (A) Enumeration of peripheral WBCs, RBCs, hemoglobin (Hb), MCV, and platelet in primary *Vav*-Cre-negative *Asxl1*-MT^{fl/wt} (control, 70 wk old, white circle, $n = 8$) and *Vav*-Cre-positive *Asxl1*-MT^{fl/wt} mice (KI, 70 wk old, black circle, $n = 11$). (B) Related to A, showing the absolute number of each lineage in the PB as determined by flow cytometry analysis. (C) Proportion of CD11b⁺Gr1⁺ cells in BM from *Vav*-Cre-negative *Asxl1*-MT^{fl/wt} (control, 12 wk old, $n = 6$) and *Vav*-Cre-positive *Asxl1*-MT^{fl/wt} mice (KI, 12 wk old, $n = 6$). (D) Flow cytometry analysis of erythroid maturation with Ter119 and CD71 antibody in the BM cells in both group in primary *Vav*-Cre-negative *Asxl1*-MT^{fl/wt} (control, 12 wk old, white bar, $n = 12$) and *Vav*-Cre-positive *Asxl1*-MT^{fl/wt} (KI, 12 wk old, black bar, $n = 12$). (E) Comparison of spleen and liver weight and BM cell number in both group in *Vav*-Cre-negative *Asxl1*-MT^{fl/wt} (control, 12 wk old; spleen and liver, $n = 6$; BM, $n = 5$) and *Vav*-Cre-positive *Asxl1*-MT^{fl/wt} mice (KI, 12 wk old; spleen and liver, $n = 6$; BM, $n = 5$). (F and G) H&E staining of BM (F) and cytopsin samples representing morphological abnormalities (G) in 70-wk-old *Vav*-Cre-positive *Asxl1*-MT^{fl/wt} BM. Arrows in F indicate megakaryocytes. Bars: 50 μm (F) and 10 μm (G). Data are presented as mean \pm SEM. *, $P < 0.05$; **, $P < 0.01$; ***, $P < 0.001$ (Student's t test).

Fig. 3 D; Murphy et al., 2013), which is consistent with the increased megakaryocytes and platelets shown in Fig. 2 (A and F) and Fig. S1 D. In line with myeloid skewing in the PB and with fewer HSCs in the BM, total colonies, erythroid CFU (CFU-Es), and erythroid burst-forming units (BFU-Es) were profoundly reduced in KI cells, whereas the number of granulocyte-macrophage CFU (CFU-GM) colonies was increased when we started

with whole BM cells (Fig. 3, E and G). To exclude the possibility that the colony output might be affected by the reduction of HSPCs shown in Fig. 3 B, we repeated the assay using the same number of LT-HSC and MPP and confirmed the reduction of BFU-Es and the increase of CFU-GMs (Fig. 3 F). In contrast to the result of whole BM cells, the total number of colonies from LT-HSC and MPP was enhanced because of dramatic changes in

CFU-GMs (Fig. 3 G). Of note, ectopic expression of ASXL1-WT in Lin[−] cells completely or partially rescued the reduction of BFU-Es/CFU-Es found in KI cells (Fig. 3, H and I). However, CFU-GMs decreased after WT expression (Fig. 3, H and I), suggesting the opposite effect of WT and mutant protein on erythroid and myeloid colony formation.

We next performed a competitive repopulation assay to determine whether expression of *Asxl1* mutant affects HSC self-renewal and reconstitution in vivo (Fig. 4 A). This revealed that *Asxl1*-MT KI mice had a significant competitive disadvantage in PB and whole BM cells (Fig. 4, B and C). Although engraftment of B220⁺ cells was severely impaired, the proportion of CD11b⁺ cells from KI donor cells was substantial (Fig. S2 A). Chimerism in whole BM cells, Lin[−] BM cells, MPs, common myeloid progenitors (CMPs), granulocyte/macrophage progenitors (GMPs), and short-term repopulating HSC fractions was severely reduced, as observed in PB cells (Fig. 4 C). In contrast, however, the donor-derived chimerism, frequency, and absolute numbers of LSK, LT-HSC, and MPP populations were not impaired in KI mice relative to controls (Fig. 4, C and D; and Fig. S2 B). In another competitive (Fig. S2 C) and a noncompetitive repopulation assay, *Asxl1* KI cells had impaired and delayed repopulation, respectively (Figs. 4 E and S2 D). The recipient mice with KI cells showed an increased proportion of myeloid cells relative to control (Figs. 4 F and S2 E). Overall, these data reveal that *Asxl1* mutant expression compromised the quality and quantity of stem cell fraction without affecting the survival of HSCs in vivo.

Mutant *RUNX1* promoted MDS/AML development in the *Asxl1* mutant background

No Vav-cre *Asxl1*-MT KI mice developed AML after long-term follow up (18 mo), suggesting that *Asxl1* mutant clones might require additional mutation for full transformation. Recent work has identified that mutations in *ASXL1* and *RUNX1* tend to coexist frequently in MDS as well as AML (Papaemmanuil et al., 2013; Chen et al., 2014; Haferlach et al., 2014). Similarly, across a cohort of 368 patients with de novo World Health Organization 2008-defined MDS (Vardiman et al., 2009) where *ASXL1* was mutated in 17.4% (64/368), patients with *ASXL1* mutation had a significantly higher incidence of concurrent *RUNX1* mutations than their *ASXL1* WT counterparts (19/64 [29.7%] vs. 20/304 [6.6%]; $P < 0.01$; Fig. 5 A). None of these *RUNX1* mutations were found to be germline line mutations in this cohort. *ASXL1/RUNX1* comutation in MDS was associated with poor overall and progression-free survival (Fig. 5 B). Prior work has demonstrated that *RUNX1* mutations can be classified into missense mutations in the N-terminal Runt domain and C-terminal truncated type mutations resulting from missense or frameshift mutations (Harada and Harada, 2009). As shown in Fig. 5 A, regardless of *ASXL1* mutational status, *RUNX1* mutations were more commonly found to be the C-terminal truncation type, such as the *RUNX1*-S291fsX mutation, rather than missense mutations in the Runt domain. Based on these findings, we next examined the in vivo effect of expression of *RUNX1*-S291fsX in the *Asxl1*-MT KI or *Asxl1* WT background. Intriguingly, mice transplanted with BM cells expressing both *Asxl1* and *RUNX1* mutations developed macrocytic anemia over

time (Figs. 5 C and S2 F) and died of MDS/AML with remarkable hepatosplenomegaly after a short latency (median survival, 160 d), whereas all of the mice transplanted with BM cells expressing only *RUNX1*-S291fsX survived for 1 yr (Fig. 5, D and E). Frequent myeloid cells with dysplastic feature were evident in the BM, spleen, and PB of the double-mutant animals with infiltration of these cells into the liver and spleen (Fig. 5, F and G). In addition, leukemic cells from mice with both *RUNX1*-S291fsX and *Asxl1*-MT KI were serially transplantable into sublethally irradiated recipients (not depicted). Coexpression of *RUNX1*-S291fsX increased the LSK fraction (Fig. 5 H). An increase in CMPs (Lin[−]c-Kit⁺Sca1[−]CD34⁺FcyR[−]) with decreased MEPs in *Asxl1/RUNX1* double mutants was compatible with the AML phenotype observed in this model (Fig. 5 H). Interestingly, we observed the more significant effects of *RUNX1* mutant expression on LT-HSC and MPP2 (CD150⁺CD48⁺LSK) rather than on LSK (Fig. 5 I; Pietras et al., 2015). Moreover, apoptosis was significantly reduced by *RUNX1* mutant expression in KI mice, which presumably contributed to the transformation, although cell cycle arrest was found in LSK and progenitors of the mice with both mutations, as previously described in *Runx1* mutant-expressing cord blood cells (Goyama et al., 2013; Fig. S2, G and H). CFU-GM and BFU-E colony output of *Asxl1*-MT KI cells was enhanced by *RUNX1*-S291fsX, whereas the CFU-E number was significantly decreased (Fig. 5 J). These data reveal that expression of mutant *RUNX1* in *Asxl1*-MT KI mice increased the stem cell fractions of the KI mice and induced myeloid leukemia at the expense of erythroid lineage maturation.

KI mice are susceptible to leukemia from insertional mutagenesis

To further assess the susceptibility of KI mice to leukemia, we applied retrovirus-mediated insertional mutagenesis by using MOL4070LTR retrovirus (MOL4070A; Wolff et al., 2003; Ikeda et al., 2016; Ueda et al., 2016), which integrates into the mouse genome and up-regulates expression of the neighboring genes. During a 1.5-yr observation period, all of MOL4070A-infected KI mice developed acute leukemia (Fig. 5 K). Macroscopically, most of the diseased *Asxl1*-MT KI + MOL4070A mice exhibited massive hepatosplenomegaly and immature myeloid blasts in terms of morphology of BM and spleen cells (Fig. 5, L and M). Most of the GFP⁺ BM cells were positive for CD11b and c-Kit, suggesting that leukemic cells derived from *Asxl1* mutant-expressing immature myeloid cells (Fig. S2 I). We detected the genomic location of integration by inverse PCR of six recipients' BM cells (Table 1). As retroviral common integration sites, we identified *Hhex*, *Rnf220*, and *H2-Eb2* across recipients. We also observed integration near *Setbp1* gene in a single recipient. This matched our previous result showing *ASXL1*-mutated MDS collaborates with *SETBP1* mutation, which impairs ubiquitin-proteasome dependent degradation of SETBP1 protein, during leukemic transformation (Inoue et al., 2015). Moreover, MLL-AF9 fusion oncogene-induced AML was enhanced in the *Asxl1*-MT KI background over *Asxl1* WT background (57 d vs. 51 d, median survival; $P = 0.0179$, log-rank test; Fig. 5 N). Overall, these in vivo results indicate that KI cells require further oncogenic alterations for leukemic transformation.

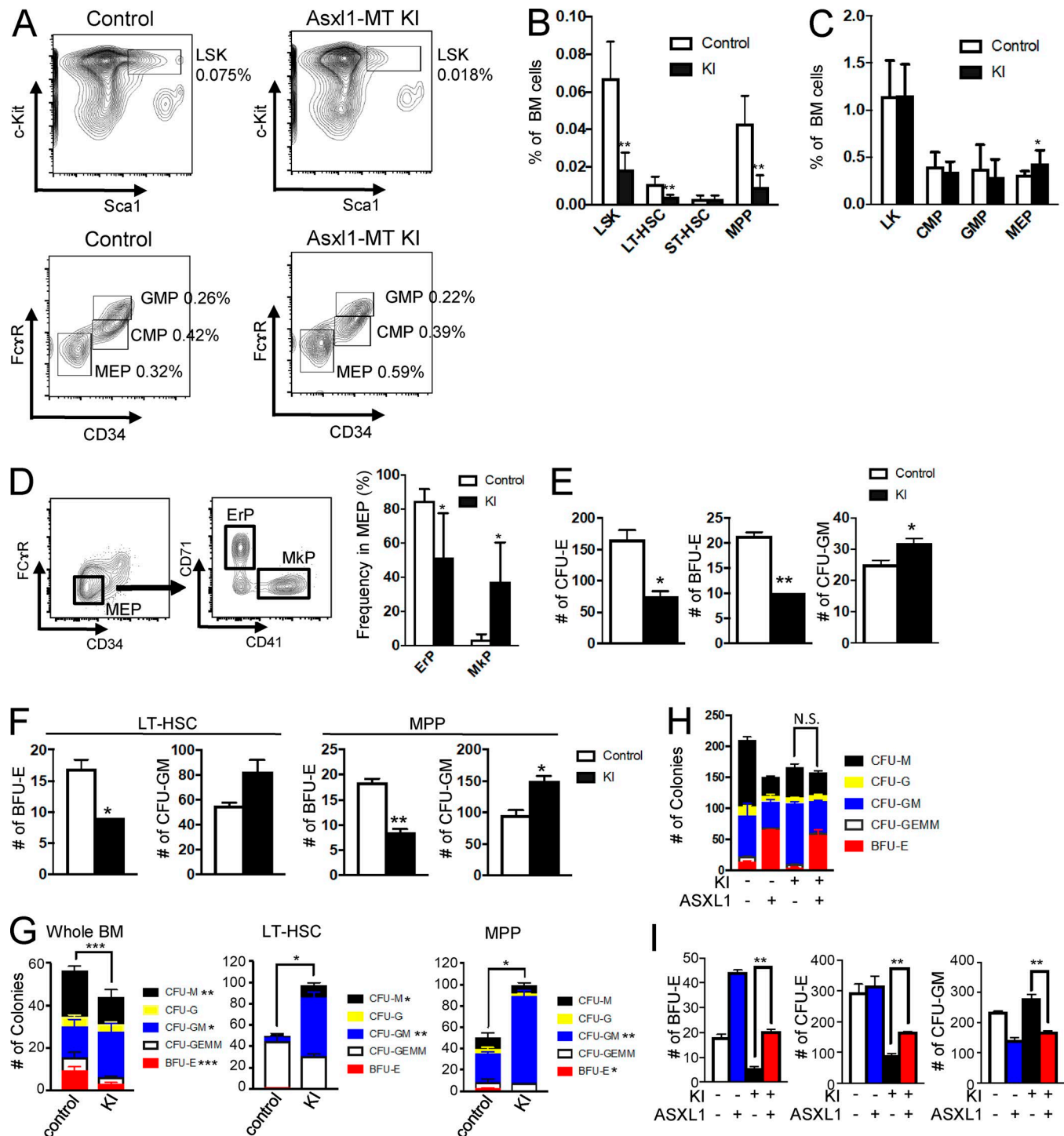


Figure 3. Functional analysis of HSCs in KI mice. (A) Flow cytometric enumeration of LSK, GMP, CMP, and MEP cells in the BM of 4-mo-old *Vav*-Cre-negative *Asxl1-MT^{fl/fl}* (control) and *Vav*-Cre-positive *Asxl1-MT^{fl/fl}* (KI) mice. (B and C) Proportion of LSK, LT-HSCs, short-term (ST) repopulating HSCs, MPPs, Lin⁻c-Kit⁺, CMPs, GMPs, and MEPs in both mice ($n = 5$ in B and $n = 8$ in C). The data are expressed as relative values (percentage), with whole BM cells being 100%. (D) Flow cytometry analysis of CD41^{low}CD71^{high} (ErP) and CD41^{high}CD71^{low} (MkP) cells from MEP cell populations (Lin⁻c-Kit⁺CD34⁻FcyR⁻) of primary *Vav*-Cre-negative *Asxl1-MT^{fl/fl}* (control, 70 wk old, white circle, $n = 5$) and *Vav*-Cre-positive *Asxl1-MT^{fl/fl}* mice (KI, 70 wk old, black circle, $n = 5$). The frequency in MEPs is shown. (E) Absolute number of colonies (BFU-E, CFU-E, and CFU-GM) from whole BM cells of *Vav*-Cre-negative *Asxl1-MT^{fl/fl}* (control) and *Vav*-Cre-positive *Asxl1-MT^{fl/fl}* (KI) mice. For the CFU-E and BFU-E assay, 10^5 and 2×10^4 BM cells per well were used, respectively. For the CFU-GM assay, 2×10^4 BM cells per well were used. Duplicate samples were plated. (F) Absolute number of colonies (BFU-E and CFU-GM) from 250 LT-HSC and MPP cells per well of *Vav*-Cre-negative *Asxl1-MT^{fl/fl}* (control) and *Vav*-Cre-positive *Asxl1-MT^{fl/fl}* (KI) mice. Duplicate samples were plated. (G) Absolute number of colonies in the M3434 condition. A total of 2×10^4 whole BM cells per well and 250 LT-HSC or MPP cells per well were used. (H and I) Absolute number of colonies with or without ASXL1 expression in the M3434 condition (H) and the BFU-E, CFU-E, and CFU-GM condition (I). We sorted the Lin⁻ fraction using MACS and retrovirally transduced empty vector (pMYs-IRES-hNGFR) and ASXL1-WT (pMYs-ASXL1-IRES-hNGFR) into Lin⁻ control or KI cells. Colony-formation assay was performed using FACS-sorted hNGFR⁺ cells. A total of 2×10^4 whole BM cells per well for BFU-E, CFU-GM, and M3434 colonies and 10^5 cells per well for CFU-E were used. Data are presented as mean \pm SEM. *, $P < 0.05$; **, $P < 0.01$; ***, $P < 0.001$ (Student's *t* test).

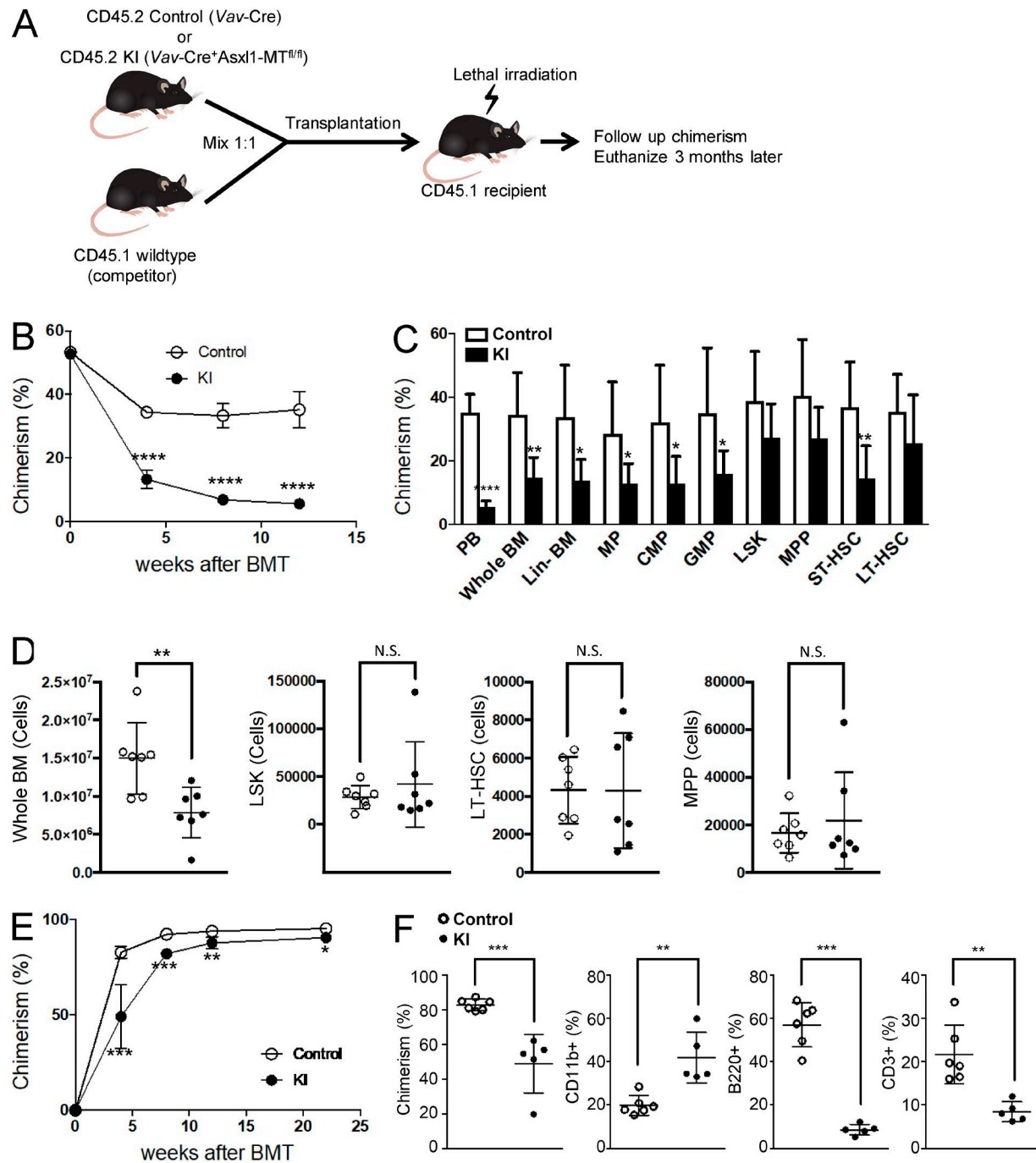
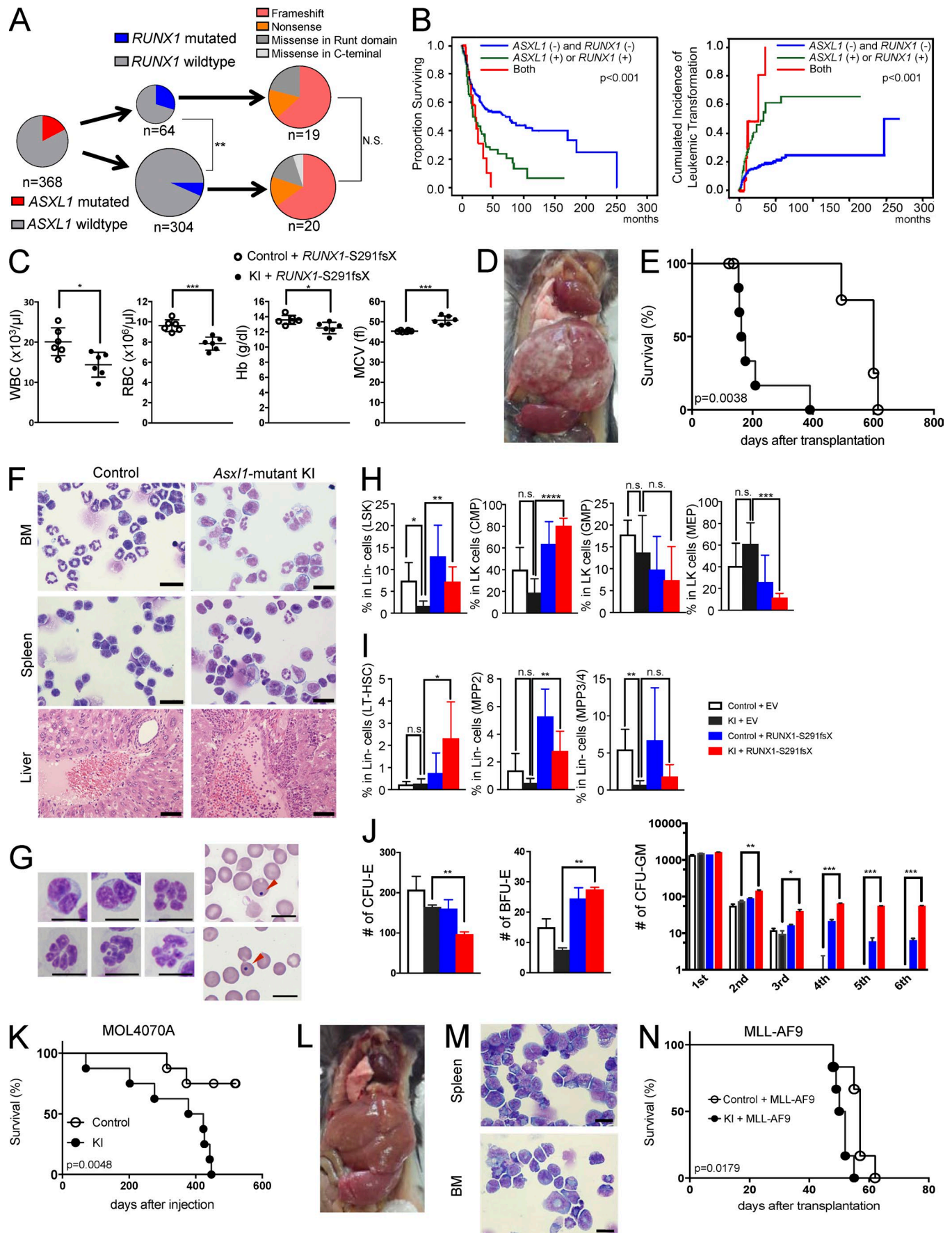


Figure 4. Competitive and noncompetitive transplantation assay. (A) Schematic depiction of the competitive transplantation assay. Vav-Cre-only and Vav-Cre-positive *Asx1-MT^{fl/fl}* mice are positive for CD45.2, whereas WT competitor cells are positive for CD45.1. Unfractionated BM cells (0.5×10^6) from CD45.2 control (Vav-Cre only) or KI (Vav-Cre-positive *Asx1-MT^{fl/fl}*) and CD45.1 WT competitor (mixed 1:1) were transplanted into lethally irradiated (9.5 Gy) recipients ($n = 7$ mice per group). We followed up the chimerism (CD45.2⁺) and CD11b/B220/CD3-positive cells in the PB every 4 wk. (B) Percentage of donor chimerism in the PB after competitive repopulation assay ($n = 7$ mice per group). (C) The donor chimerism (CD45.2⁺) of each stem/progenitor fraction was evaluated by FACS. ST, short term. (D) The absolute number of CD45.2⁺ whole BM, LSK, LT-HSCs, and MPPs in each group ($n = 7$ each). (E) Percentage of donor chimerism in the PB 4–22 wk after noncompetitive repopulation assay. Unfractionated BM cells (10^6) from control (Vav-Cre-negative *Asx1-MT^{fl/wt}*) or KI (Vav-Cre-positive *Asx1-MT^{fl/wt}*) mice were used as donor cells ($n = 6$ in control and $n = 5$ in KI). (F) Related to E; shows the proportion of donor chimerism and each lineage in the PB at 4 wk after transplantation in a noncompetitive fashion. The cells derived from Vav-Cre *Asx1-MT^{fl/wt}* mice were identified by CD45.2 positivity. Data are presented as mean \pm SEM. *, $P < 0.05$; **, $P < 0.01$; ***, $P < 0.001$; ****, $P < 0.0001$ (Student's *t* test). All of the control mice used in the transplantation assay were age matched. BMT, bone marrow transplantation.



Transcriptional and epigenetic alterations in mutant *Asxl1* progenitors

To understand the basis for the impaired erythroid differentiation and stem cell dysfunction observed in *Asxl1*-MT KI mice, we performed RNA-seq of sorted c-Kit⁺ BM cells from 2.5-mo-old KI mice and age-matched littermate controls. In line with previous studies, *Hoxa9* was up-regulated in KI cells and gene set enrichment analysis (GSEA) demonstrated gene sets containing *Hoxa9*, and *Myc* target genes were enriched in c-Kit⁺ BM cells from KI mice compared with controls (Schuhmacher et al., 2001; Hess et al., 2006), whereas GATA-binding protein 1 (GATA1) or RUNX1 targets (Suzuki et al., 2009, 2013), both of which are known to contribute to erythroid differentiation (Yokomizo et al., 2008; Suzuki et al., 2013), were repressed in KI mice (Fig. 6 A). Consistent with the data shown in Fig. 3 C, c-Kit⁺ KI cells showed significant loss of gene sets enriched in HSC against MEPs (Ng et al., 2009), whereas genes involved in erythroid differentiation and heme metabolism were inhibited (Figs. 6 A and S3 A; Addya et al., 2004; Riz et al., 2007). Of note, the gene sets enriched in HSCs relative to MEPs and the targets of RUNX1 and GATA1 were also significantly down-regulated in LSK fractions of KI mice compared with those of control mice, which support our results regardless of cell population analyzed (Suzuki et al., 2009, 2013; Fig. S3 B). We also compared RNA-sequencing data from KI mice with those of LSK cells from *Asxl1* KO mice (Abdel-Wahab et al., 2013). There were 939 and 266 genes commonly up-regulated and down-regulated across both models, respectively (Fig. 6 B). Gene ontology (GO) biological process enrichment analysis identified the common ontologies related to RNA splicing, ribosome, erythroid/myeloid differentiation, immune activation, and kinase activation in gene sets commonly dysregulated or differentially expressed only in KI cells (Figs. 6 C and S3 C).

Previous studies have associated *Asxl1* loss or mutant over-expression with loss of histone H3 lysine 27 trimethylation (H3K27me3) as well as decreased H2A lysine 119 monoubiquitination (H2AK119Ub) caused by alterations in PRC2 and BAP1 function, respectively, in *ASXL1* mutant cells (Abdel-Wahab et

al., 2012; Inoue et al., 2013; Wang et al., 2014; Balasubramani et al., 2015). However, these potential effects of *ASXL1* alterations on chromatin state have not been investigated with physiological expression of mutant *Asxl1* previously. We therefore performed anti-H3K4me3 (H3 lysine 4 trimethylation), H3K27me3, and H2AK119Ub chromatin immunoprecipitation (ChIP) followed by next-generation sequencing (ChIP-seq) in c-Kit⁺ BM cells from KI mice and littermate controls. Consistent with the result of Western blot analysis (Fig. 6 D), H3K4me3 and H2AK119Ub were globally decreased in *Asxl1*-MT KI cells relative to controls, whereas H3K27me3 was not significantly affected (Figs. 6 E and S3 D). However, evaluation of site-specific abundance of histone modifications at the *Hoxa* loci revealed reductions in H3K27me3 (Fig. 6 F), which were focal and not global, and there was no correlation between EZH2 target genes and genes dysregulated in *Asxl1*-MT KI mice (Fig. 6 A; Kamminga et al., 2006). Given that reductions in H3K4me3, a mark associated with active gene expression, were the most apparent histone modification change in *Asxl1*-MT KI cells, we evaluated genes that had particularly strong reductions in H3K4me3 in the KI cells. Such sites were identified at *Sox6*, *inhibitor of DNA binding 3 (Id3)*, *Tjp1*, and *Hba* loci, whose mRNA expression levels were validated in quantitative RT-PCR (Fig. 6, F and G; and Fig. S3 E) and all of which encode proteins involved in erythroid differentiation and/or maturation (Deed et al., 1998; Cantù et al., 2011; Zhao et al., 2016). Changes in H3K4me3 abundance were positively correlated with gene expression changes and negatively correlated with H2AK119Ub changes, whereas changes in H2AK119Ub abundance were negatively correlated with gene expression changes (Fig. S3 F). We therefore next investigated whether H3K4me3 loss occurred in a specific manner. The reduction of H3K4me3 can be observed independently of transcribed levels as shown in Fig. S3 G, where we classified protein-coding genes into four categories based on expression levels. Next, we focused on loci marked by both H3K4me3 and H2AK119Ub in control cells. Within the overlapped peaks, we classified these into four groups; (1) both modifications remained in KI (4,468 peaks), (2) only H3K4me3

Figure 5. Mutant KI increased susceptibility to leukemic transformation. (A) Proportion of *RUNX1* mutations among *ASXL1*-mutated (left, $n = 64$) or *ASXL1*-WT (right, $n = 304$) MDS patients and types of *RUNX1* mutations in each group. Statistical significance was evaluated by chi-square test. (B) Kaplan-Meier analysis for survival (left) and cumulative incidence of leukemic transformation (right) depending on mutational status of *ASXL1* and *RUNX1* in MDS patients. (C) Enumeration of peripheral WBCs, RBCs, hemoglobin (Hb), and MCV in mice transplanted with *RUNX1*-S291fsX-transduced *Vav*-Cre-negative *Asxl1*-MT^{fl/wt} (control + *RUNX1*-S291fsX, white circle, $n = 6$) or *Vav*-Cre-positive *Asxl1*-MT^{fl/wt} 3 mo after transplantation (KI + *RUNX1*-S291fsX, black circle, $n = 6$). (D) Representative hepatosplenomegaly in the KI group. (E) Kaplan-Meier analysis for the survival of transplanted mice ($n = 6$ each). (F) Cytospin preparations of BM (top) and spleen (middle) and pathological analysis of liver (bottom) from control and KI group. Bars: 20 μ m (top and middle) and 50 μ m (bottom). (G) Morphological abnormality of PB cells found in KI group 3 or 4 mo after transplantation. Howell-Jolly bodies are indicated by arrows (right). Bars, 10 μ m. (H) Proportion of LSK in Lin⁻ cells and CMPs, GMPs, and MEPs in Lin⁻c-Kit⁺ BM cells of the recipient mice transplanted with control (*Vav*-Cre-negative *Asxl1*-MT^{fl/wt}) plus empty vector (white, $n = 3$), KI (*Vav*-Cre-positive *Asxl1*-MT^{fl/wt}) plus empty vector (black, $n = 5$), control plus *RUNX1*-S291fsX (blue, $n = 6$), or KI plus *RUNX1*-S291fsX mutation (red, $n = 6$). (I) Proportion of LT-HSC and MPP2 (CD150⁺CD48⁺LSK), MPP3/4 (CD150⁺CD48⁺LSK) in Lin⁻ BM cells of the recipient mice transplanted with control (*Vav*-Cre-negative *Asxl1*-MT^{fl/wt}) plus empty vector (white, $n = 3$), KI (*Vav*-Cre-positive *Asxl1*-MT^{fl/wt}) plus empty vector (black, $n = 4$), control plus *RUNX1*-S291fsX (blue, $n = 4$), or KI plus *RUNX1*-S291fsX mutation (red, $n = 4$). All mice were euthanized 3 mo after transplantation. (J) Absolute number of colonies (BFU-Es, CFU-Es, and CFU-GMs) using control or KI BM cells infected with or without the *RUNX1*-S291fsX mutation. For the CFU-E and BFU-E assay, 10^5 and 2×10^4 BM cells per well were used, respectively. For the CFU-GM assay, 2×10^4 BM cells per well were used and replated similarly every week. The color of bars represents the same group shown in I. Duplicate samples were plated. (K) Kaplan-Meier analysis for the survival after injection of MOL4070A (control, white circle, $n = 8$ and KI, black circle, $n = 8$). (L) Representative hepatosplenomegaly in KI mice plus MOL4070A group. (M) Cytospin preparations of spleen (top) and BM (bottom) cells derived from mice with KI mice plus MOL4070A. Bars, 20 μ m. (N) *Asxl1*-MT KI accelerated MLL-AF9 induced leukemia. Kaplan-Meier curve for the survival of the mice transplanted with MLL-AF9-transduced control (*Vav*-Cre-negative *Asxl1*-MT^{fl/wt}) and KI (*Vav*-Cre-positive *Asxl1*-MT^{fl/wt}) BM cells ($n = 6$ each) are shown. Data are presented as mean \pm SEM. *, $P < 0.05$; **, $P < 0.01$; ***, $P < 0.001$; ****, $P < 0.0001$ (Student's t test). Log-rank test was used to compare the survival distributions of two samples.

Table 1. Retrovirus integration sites identified by inverse PCR

Mouse no.	Gene name	Genome position	Integration site	Gene description
1	<i>Ly6e</i>	chr15(qD3)	20 kb up	Lymphocyte antigen 6 complex, locus E
	<i>Fgd2</i>	chr17(qA3,3)	15 kb down	FYVE, RhoGEF, and PH domain containing 2
	<i>H2-Eb2^a</i>	chr17(qB1)	Intron 1	Histocompatibility 2, class II antigen E beta2
	<i>Fn1</i>	chr1(qC3)	200 kb down	Fibronectin 1
	<i>Acvrl1</i>	chr15(qF1)	10 kb down	Activin A receptor, type II-like 1
	<i>Rab37</i>	chr11(qE2)	Intron 1	RAB37, member RAS oncogene family
	<i>Pitpnc1</i>	chr11(qE1)	Intron 1	Phosphatidylinositol transfer protein, cytoplasmic 1
	<i>Zfp541</i>	chr7(qA2)	15 kb up	Zinc-finger protein 541
	<i>Numb</i>	chr12(qD1)	15 kb up	Numb homologue (<i>Drosophila</i>)
	<i>Irf8</i>	chr8(qE1)	50 kb down	Interferon regulatory factor 8
	<i>Rnf220^a</i>	chr4(qD1)	Intron 2	Ring-finger protein 220
	<i>Fcnb</i>	chr2(qA3)	10 kb up	Ficolin B
	<i>Padi2</i>	chr4(qD3)	1 kb up	Peptidyl arginine deiminase, type II
	<i>Kctd12</i>	chr14(qE2,3)	100 kb down	Potassium channel tetramerization domain containing 12
	<i>Myb</i>	chr10(qA3)	Intron 9	Myeloblastosis oncogene
	<i>Hhex^a</i>	chr19(qC2)	50 kb down	Hematopoietically expressed homeobox
2	<i>Arpc3</i>	chr5(qF)	Intron 2	Actin-related protein 2/3 complex, subunit 3
	<i>Setbp1</i>	chr18(qE3)	200 kb up	SET-binding protein 1
	<i>Mlap</i>	chr(qC3)	Exon 1 (5' UTR)	Meiosis 1-associated protein
	<i>Ift81</i>	chr5(qF)	10 kb up	Intraflagellar transport 81
3	<i>Cmb1</i>	chr15(qB2)	0.2 kb up	Carboxymethylenebutenolidase-like (<i>Pseudomonas</i>)
	<i>Gsn</i>	chr2(qB)	10 kb up	Gelsolin
	<i>Qars</i>	chr9(qF2)	Intron 1	Glutamyl-tRNA synthetase
	<i>Rbbp6</i>	chr7(qF2)	20 kb up	Retinoblastoma-binding protein 6
	<i>Prdm16</i>	chr4(qE2)	Intron 1	PR domain containing 16
	<i>Mkln1</i>	chr6(qA3,3)	200 kb up	Muskelin 1, intracellular mediator containing kelch motifs
	<i>Fhad1</i>	chr4(qE1)	Intron 13	Forkhead-associated phosphopeptide binding domain 1
	<i>Rassf2</i>	chr2(qF2)	Intron 1	Ras association (RalGDS/AF-6) domain family member 2
	<i>Neurl1b</i>	chr17(qA3,3)	20 kb up	Neuralized E3 ubiquitin protein ligase 1B
	<i>Rnf220^a</i>	chr4(qD1)	Intron 2	Ring finger protein 220
	<i>EV1</i>	chr12(qF1)	Intron 1	Ena-vasodilator stimulated phosphoprotein
	<i>Ubash3a</i>	chr17(qA3,3)	Intron 6	Ubiquitin associated and SH3 domain containing, A
	<i>Pcbp1</i>	chr6(qD1)	20 kb down	Poly(rC) binding protein 1
4	<i>Fggy</i>	chr4(qC5)	200 kb up	FGGY carbohydrate kinase domain containing
	<i>Adgre5</i>	chr8(qC2)	Intron 1	Adhesion G protein-coupled receptor E5
	<i>Smim19</i>	chr8(qA2)	Exon 5 (3' UTR)	Small integral membrane protein 19
	<i>Igch</i>	chr9(qC)	Intron 13	IQ motif containing H
	<i>Pim1</i>	chr17(qA3,3)	1 kb up	Proviral integration site 1
	<i>Serpina3j</i>	chr12(qE)	Intron 2	Serine (or cysteine) peptidase inhibitor, clade A (alpha-1 antiproteinase, antitrypsin), member 3j
	<i>Katnal1</i>	chr5(qG3)	50 kb up	Katanin p60 subunit A-like 1
	<i>H2-Eb2^a</i>	chr17(qB1)	Intron 1	Histocompatibility 2, class II antigen E beta2

Table 1. Retrovirus integration sites identified by inverse PCR (Continued)

Mouse no.	Gene name	Genome position	Integration site	Gene description
5	<i>Rere</i>	chr4(qE2)	Intron 11	Arginine glutamic acid dipeptide (RE) repeats
	<i>B3gnt2</i>	chr11(qA3,2)	Intron 1	UDP-GlcNAc:betaGal beta-1,3-N-acetylglucosaminyltransferase 2
	<i>Casp8</i>	chr1(qC1,3)	Intron 1	Caspase-8
	<i>Hhex^a</i>	chr19(qC2)	20 kb down	Hematopoietically expressed homeobox
	<i>Fam76a</i>	chr4(qD2,3)	20 kb up	Family with sequence similarity 76, member A
	<i>Rhoh</i>	chr5(qC3,1)	50 kb down	ras homologue family member H
	<i>Xxylt1</i>	chr16(qB2)	Intron 3	Xyloside xylosyltransferase 1
6	<i>Tmprss4</i>	chr9(qA5,2)	Intron 1	Transmembrane protease, serine 4
	<i>Rras2</i>	chr7(qF1)	50 kb up	Related RAS viral (r-ras) oncogene 2
	<i>Adrbk2</i>	chr5(qF)	Intron 1	Adrenergic receptor kinase, beta 2
	<i>Stx6</i>	chr1(G3)	5 kb up	Syntaxin 6
	<i>Ets2</i>	chr16(qC4)	100 kb down	E26 avian leukemia oncogene 2, 3' domain
	<i>Tmprss4</i>	chr9(qA5,2)	Intron 1	Transmembrane protease, serine 4
	<i>Pla2g15</i>	chr8(qD3)	Intron 1	Phospholipase A2, group XV
	<i>Zmiz1</i>	chr14(qA3)	50 kb up	Zinc finger, MIZ-type containing 1
	<i>Brip1os</i>	chr11(qC)	Intron 1	BRCA1-interacting protein C-terminal helicase 1, opposite strand
	<i>Ephb2</i>	chr4(qD3)	Exon 1 (5' UTR)	Eph receptor B2
	<i>Plin3</i>	chr17	1 kb up	Perilipin 3

^aRetroviral common integration site.

remained in KI (1,236 peaks), (3) only H2AK119Ub remained in KI (185 peaks), and (4) both modifications absent in KI (80 peaks; Fig. S4 A). Of note, even in group 2, where H2AK119Ub disappeared in KI cells, H3K4me3 signals were also reduced in KI cells. Similarly, in group 3, where H3K4me3 disappeared in KI cells, H2AK119Ub signals decreased but H3K27me3 signals increased in KI cells (Fig. S4 B). These data suggest profound effects of Asxl1 mutant on the reduction of both H3K4me3 and H2AK119Ub even in genes with both modifications. We used the above genomic data to identify mutant Asxl1 target genes and evaluate whether any of these possible targets rescue the phenotype of *Asxl1*-MT KI BM cells. ID3 is a previously described target of WT ASXL1 and RUNX1, and its expression or loss promotes or inhibits erythropoiesis, respectively (Deed et al., 1998; Abdel-Wahab et al., 2013; Zhao et al., 2016). *Id3* expression was down-regulated in *Asxl1*-MT KI cells associated with reduced H3K4me3 at the *Id3* locus (Fig. 6 F). Remarkably, reexpression of *Id3* in *Asxl1*-MT KI BM cells rescued CFU-E and BFU-E numbers (Fig. 6 H). These results suggest that H3K4me3 reduction around *Id3* resulted in transcriptional repression and, at least in part, is responsible for the maturation block in erythroid lineage.

Effects of genome-wide binding of WT versus mutant ASXL1 on histone modifications

Next, to examine the potential effects of WT and mutant Asxl1 binding on H3K4me3, we performed ChIP-seq with N-terminal Asxl1 and FLAG antibody using c-Kit⁺ control (WT) and KI BM cells. Nearly all mutant (FLAG) binding sites were shared with

Asxl1-WT binding sites (2,365 of 2,520 genes, 93.8%), compatible with a study showing that the predicted DNA-binding region of ASXL1 is located in its N terminus (Sanchez-Pulido et al., 2012; Fig. 7 A). Although mutant binding sites were more enriched at promoter regions than WT binding sites (Fig. 7 B), binding motif enrichment analysis of WT and FLAG (mutant) ChIP-seq revealed similar results, including a variety of E-twenty six (ETS) transcriptional factors (Table S1). In fact, *Id3* gene was identified as the target of both Asxl1-WT and mutant (Fig. 7 C), suggesting Asxl1 is directly involved in *Id3* expression. Next, we investigated how WT Asxl1 affects global H3K4me3, H3K27me3, and H2AK119Ub levels. Intriguingly, the intensity of Asxl1 binding in control cells was well correlated with H3K4me3 ($R^2 = 0.75$) and H2AK119Ub ($R^2 = 0.4$) abundance, but not that of H3K27me3 ($R^2 = 1.1e-05$), indicating that Asxl1 itself supports H3K4me3 and H2AK119Ub modification (Fig. 7 D). Asxl1 WT binding signals tend to correlate with the ratio of H3K4me3 to H3K27me3 (Fig. 7 E), although H3K27me3 was decreased at specific loci, such as the posterior *Hox A* locus, without global reduction (Fig. 6 F). Combined with ChIP-seq analyses for H3K4me3, we demonstrated that the intensity of Asxl1 mutant (FLAG) binding tends to be correlated with the reduction of H3K4me3 in KI mice (Fig. 7 F). Given that WT and mutant share the same targets, these data strongly suggest that WT supports H3K4me3 modification, but mutant does not. Moreover, motif enrichment analysis of differential H3K4me3 peaks in KI versus WT revealed enrichment of motifs characteristic of ETS family of transcription factors (TFs; Fig. 7 G), similar to the binding motifs of both WT and mutant

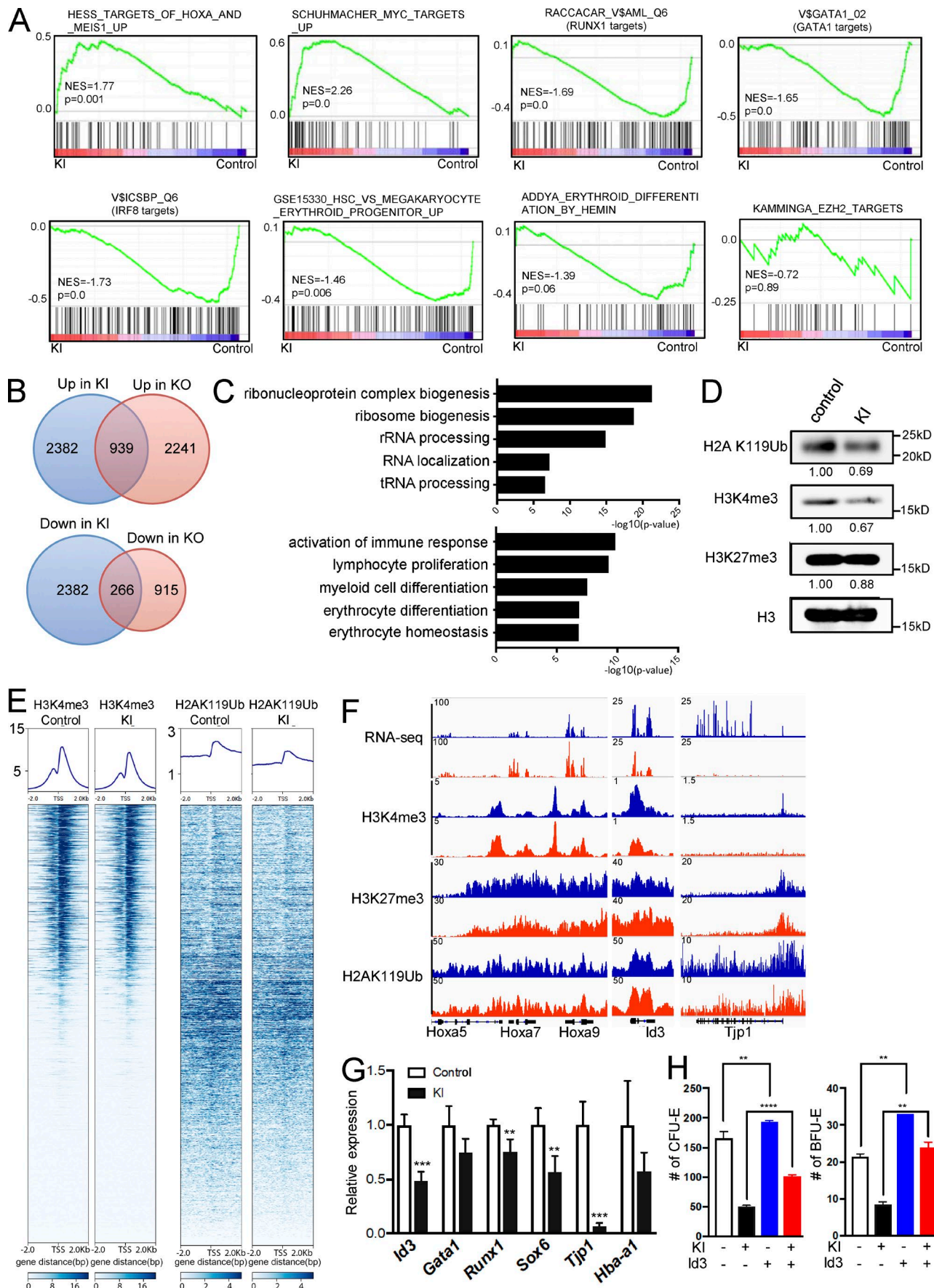


(Table S1; Abdel-Wahab et al., 2013). In addition, the motif of IRF8, whose targets were significantly down-regulated in KI cells (Fig. 7 G), was detected, consistent with the observation that silencing of IRF8 promotes development of “preleukemic” clones and that MDS patients with a higher risk of progression to AML had lower IRF8 levels (Will et al., 2015). Finally, we compared H3K27me3 peaks in c-Kit⁺ BM cells from KI and KO mice, which were previously reported (Fig. S4, C and D; Abdel-Wahab et al., 2013). As expected, we demonstrated that the number of genes whose promoters are modified with H3K27me3 was much larger in KI cells than in KO cells, indicating the different roles of KI and KO in H3K27me3 (Fig. S4, C and D).

Discussion

Here, we show that expression of mutant *Asx1l* in hematopoietic tissues results in myeloid skewing and age-dependent mild anemia with erythroid differentiation block, modest dysplasia, and thrombocytosis. These results are consistent with the enrichment of *ASXL1* mutations in myeloid neoplasms and the worsened anemia encountered in MDS and myeloproliferative neoplasm patients with *ASXL1* mutations (Quesada et al., 2011; Zhang et al., 2012; Shi et al., 2016). Prior models of constitutive as well as conditional *Asx1l* deletion in vivo revealed that *Asx1l* loss results in impaired HSC self-renewal (Abdel-Wahab et al., 2013; Wang et al., 2014). However, the impaired HSC self-renewal with *Asx1l* loss appears to conflict with the fact that *ASXL1* mutations are enriched in settings of clonal advantage seen in CHIP and myeloid neoplasms (Genovese et al., 2014; Jaiswal et al., 2014; Xie et al., 2014). This discrepancy, in part, has led to the hypothesis that *ASXL1* mutations may alter *ASXL1* function rather simply conferring a loss of function. Here, we have directly addressed this hypothesis by generating and characterizing mice engineered to express one of the common mutations in *ASXL1* in a conditional, hematopoietic-specific manner, although KI at *Rosa26* instead of the endogenous *Asx1l* locus cannot retain all the regulatory elements that control mutant expression. In this model, expression of mutant *Asx1l* results in an impaired quantity and quality of HSPCs, similar to what has been encountered in *Asx1l* KO mice (Abdel-Wahab et al., 2013; Wang et al., 2014). However, the chimerism of LSK and LT-HSC did not decrease in the competitive transplantation assay, whereas that of more mature progenitors as well as whole BM cells exhibited competitive disadvantage. These data indicate that *ASXL1* mutations maintain survival at the HSC level and promote transformation into MDS/AML after acquiring additional mutations, such as in *RUNX1*. One possible

hypothesis for this is that the epigenetic alterations associated with mutations in *ASXL1* might have context-specific effects depending on the cell type, resulting in distinct phenotypic effects in stem cells versus more differentiated progeny. In fact, we identified that expression of mutant *Asx1l* increases susceptibility of HSPCs to transformation by several oncogenic stimuli. For example, expression of mutant *RUNX1* rescued the disadvantage of HSPCs derived from KI mice (Fig. 5) and increased LT-HSC/MPP and reduced apoptosis in KI cells (Figs. 5 I and S2 H), suggesting that the double-mutant model can be considered a slowly progressive AML model with expanded LT-HSC/LSK/MPP populations (Fig. 5, H and I). These data suggest that *ASXL1*-mutated cells may be founder clones for human MDS/AML and that *ASXL1* mutations render HSPCs susceptible to transformation with the acquisition of additional mutations. The *RUNX1/Asx1l* double-mutant model generated here also provides a model for the one of the most adverse genotypes of AML, as recently described in the newest clinical guidelines for AML management (Döhner et al., 2017). Furthermore, we identified some common integration sites shown in Table 1. *Hhex* (hematopoietically expressed homeobox) is a direct target of Runx1 and supports PRC2-mediated repression of *Cdkn2a* in AML cells (Shields et al., 2016; Behrens et al., 2017).

Asx, the *Drosophila melanogaster* homologue of mammalian *ASXL1*-3, is required to both maintain repression and activate expression of *Hox* genes, and *ASXL* genes are thought to mediate the balance between polycomb and trithorax functions (Milne et al., 1999). More recent work has identified that *Asx* and *ASXL1/2* serve as cofactors for the H2AK119Ub deubiquitinase BAP1 (Sowa et al., 2009; Scheuermann et al., 2010; Dey et al., 2012), and mutant *ASXL1* rather than WT enhances deubiquitinase activity. Simultaneous overexpression of BAP1 and mutant *ASXL1* promotes the deubiquitinase activity of BAP1, leading to the loss of H2AK119Ub followed by H3K27me3 reduction (Balasubramani et al., 2015). At the same time, *ASXL1* loss or mutation in hematopoietic cells is associated with down-regulation of H3K27me3 (Abdel-Wahab et al., 2012; Inoue et al., 2013; Wang et al., 2014). However, the consequences of physiological *Asx1l* mutant expression have not been fully explored. Here, we first demonstrated that *ASXL1* WT binding was associated with the abundance of H3K4me3 and H2AK119Ub and that physiological expression of mutant in vivo was involved in global reductions in these modifications (Fig. 6, D–F; and Fig. 7, D–F). Balasubramani et al. (2015) used retroviral overexpression of both *ASXL1* mutant and BAP1 to show dual reduction in H2AK119Ub and H3K27me3. In our model, BAP1 mRNA did not change in KI mice, and physiological expression of *Asx1l* mutant seemed to mildly support Bap1 function, which

Figure 6. Transcriptional and epigenetic alterations in c-Kit⁺ KI cells. (A) GSEA of c-Kit⁺ cells showing gene sets positively or negatively associated with expression of mutant *Asx1l*. KI, Vav-Cre-positive *Asx1l*-MT^{fl/fl}; control, Vav-Cre-negative *Asx1l*-MT^{fl/fl}. (B) Overlap of up-regulated (top) and down-regulated (bottom) genes both in KI (blue) and KO (red) cells. (C) GO biological process enrichment analysis of up-regulated (top) and down-regulated (bottom) genes only in KI cells. (D) Anti-H2AK119Ub, H3K4me3, H3K27me3, and H3 Western blot in BM cells of control and KI mice. (E) Heatmap representation of H3K4me3 (left) and H2AK119Ub (right). ChIP-seq signals centered on TSSs. (F) RNA-seq and H3K4me3, H3K27me3, and H2AK119Ub ChIP-seq sequencing reads across the *Hoxa*, *Id3*, *Tjp1* loci in control (blue) and KI c-Kit⁺ (red) cells. (G) Quantitative RT-PCR results of the indicated genes. Control (Vav-Cre-negative *Asx1l*-MT^{fl/fl}) and KI (Vav-Cre-positive *Asx1l*-MT^{fl/fl}) c-Kit⁺ BM cells ($n = 4$ each) were used. (H) Absolute number of CFU-E and BFU-E colonies after adding back Id3 into control (Vav-Cre-negative *Asx1l*-MT^{fl/fl}) and KI (Vav-Cre-positive *Asx1l*-MT^{fl/fl}) BM cells. Data are presented as mean \pm SEM if not otherwise specified. **, $P < 0.01$; ***, $P < 0.001$; ****, $P < 0.0001$ (Student's t test). NES, normalized enrichment score.

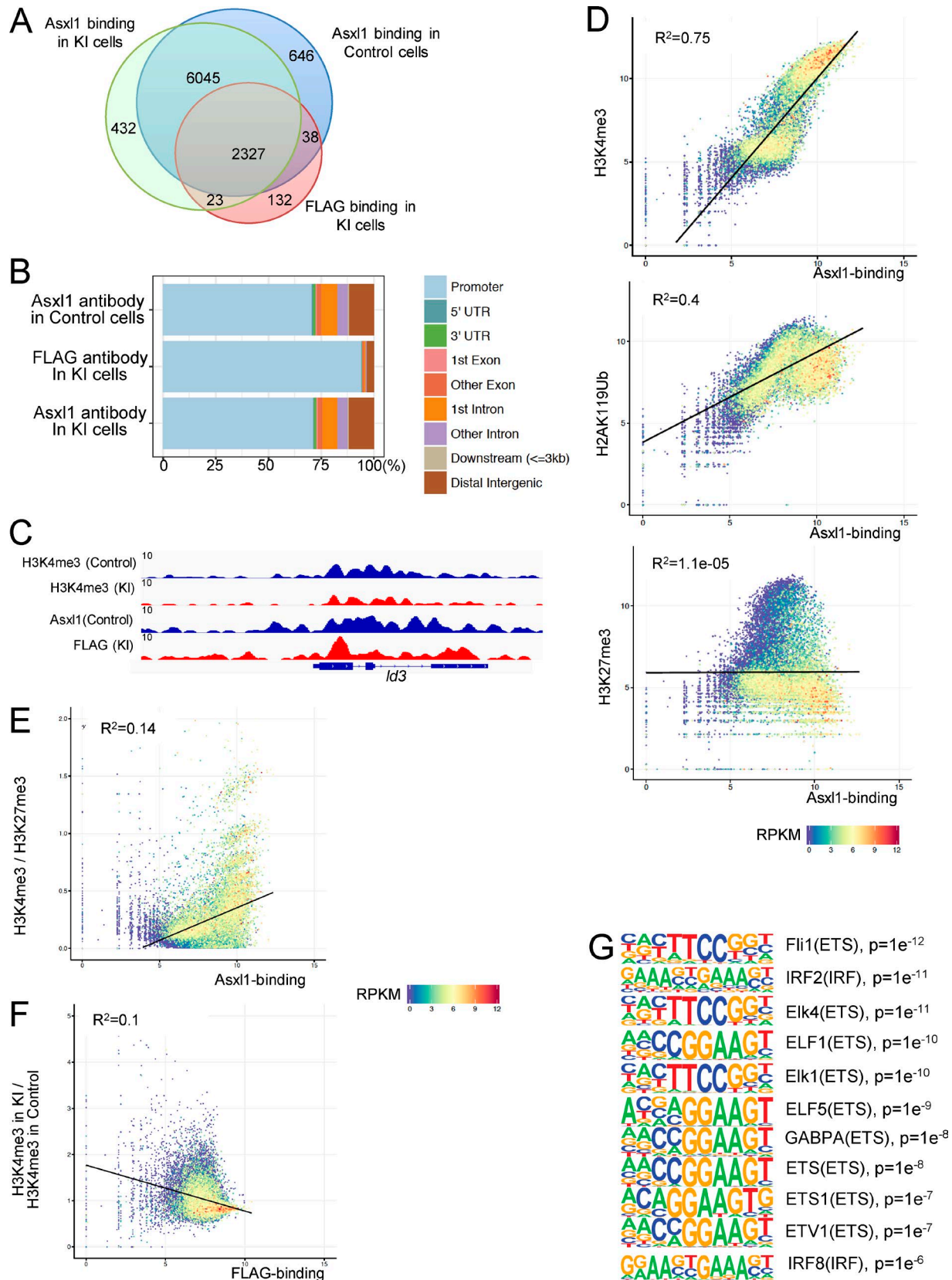


Figure 7. Effects of genome-wide binding of WT versus mutant ASXL1 on histone modifications. (A) Overlap of Asxl1- and FLAG-binding sites in c-Kit⁺ control cells and KI cells. Asxl1 antibody recognizes the N terminus of Asxl1 and binds both WT and mutant Asxl1. FLAG antibody interacts exclusively with Asxl1 mutant. (B) Bar chart showing genomic distribution of Asxl1 and FLAG (Asxl1 mutant) binding peaks relative to RefSeq functional categories, including promoters (within 5 kb upstream of TSSs), 5' untranslated regions (UTRs), exons, introns, 3' UTRs, downstream (within 5 kb downstream of the gene), and

is not sufficient for global H3K27me3 reduction. In fact, overexpression of either ASXL1 mutant or BAP1 has not been found to profoundly reduce global H3K27me3 levels.

Regarding the molecular mechanism by which ASXL1 WT supports H3K4me3 levels, we recently identified OGT (O-linked N-acetylglucosamine [GlcNAc] transferase) and HCFC1 (host cell factor C1) as interacting partners of both ASXL1 WT and mutant proteins by mass spectrometry and immunoprecipitation (Inoue et al., 2018). Previous studies identified that OGT/HCFC1 recruit trithorax homologues, including MLL, SET1/COMPASS, and MLL5 (Yokoyama et al., 2004; Tyagi et al., 2007; Deplus et al., 2013; Zhou et al., 2013). We also clarified that knockdown of ASXL1, OGT, HCFC1, or MLL5 reduces global H3K4me3 and impairs hematopoietic differentiation with robust overlap between H3K4me3-down-regulated loci with knockdown of each factor (Inoue et al., 2018). These data suggest that ASXL1 can support the methyltransferase activity of trithorax homologues through OGT/HCFC1. Considering that ASXL1 WT and mutant share the same putative DNA binding domain whereas mutant binding signals negatively correlate with H3K4me3 changes in KI mice with differential H3K4me3 peaks containing binding sites of ETS family TFs (Sanchez-Pulido et al., 2012; Abdel-Wahab et al., 2013; Fig. 7, B–G), it is tempting to speculate that Asxl1-truncated mutants may compete with WT Asxl1 to access DNA around the transcription start site (TSS) and/or to recruit H3K4 methyltransferases and ETS family TFs.

Down-regulation of gene expression and loss of H3K4me3 were apparent at genes involved in erythroid differentiation as well as targets of GATA1 and RUNX1, both of which are known regulators of erythroid maturation (Yokomizo et al., 2008; Suzuki et al., 2009, 2013). For example, reduced expression and lower levels of H3K4me3 were evident at *Id3* and *Sox6*, which play important roles in erythroid differentiation (Cantù et al., 2011; Zhao et al., 2016) and are known *Asxl1* and *Runx1* targets (Abdel-Wahab et al., 2013). Reexpression of *Id3* cDNA into *Asxl1*-MT KI BM cells could rescue the colony-forming ability of *Asxl1* mutant cells. These data suggest that *Id3* may be a key target in mediating impaired erythropoiesis in ASXL1 mutant cells. Given that *ID3* is also a target of the TGF- β pathway, evaluation of drugs targeting this pathway, which have shown promise in improving anemia in ongoing clinical trials of MDS patients based on the ASXL1 genotype of MDS patients, may be of therapeutic importance (Paulson, 2014; Blank and Karlsson, 2015).

Collectively, our experiments revealed that stable, physiological expression of mutant *Asxl1* results in dysfunction of HSPCs and perturbed erythroid-lineage differentiation. Given the paucity of mouse models for clonal hematopoiesis, we believe our model will contribute to future studies that aim to elucidate the molecular basis for MDS/AML development from precancer

clones. These results will be critically important in identifying potential novel therapies targeting cells bearing expression of mutant *Asxl1*.

Materials and methods

Patients

Adult patients ($n = 368$) with de novo MDS diagnosed according to the 2008 World Health Organization classification (Vardiman et al., 2009) at the National Taiwan University Hospital (NTUH) who had cryopreserved BM cells for study were recruited for gene mutation analyses. All patients signed informed consents for sample collection in accordance with the Declaration of Helsinki. The clinical portion of this study was approved by the institutional review board of NTUH (approval no. 201507084RINA). The coding region of *ASXL1* and *RUNX1* was amplified and sequenced as described previously (Chen et al., 2014).

Mice

A mutant mouse *Asxl1* cDNA was subcloned between a floxed neomycin resistance-stop/pA cassette and an Frt-flanked IRES-EGFP/pA cassette of STOP-eGFP-ROSA26TV, which was obtained from Y. Sasaki (Kyoto University, Kyoto, Japan) via H. Koseki (RIKEN, Yokohama, Kanagawa, Japan). Electroporation and screening of ESCs were performed as previously described (Ueda et al., 2016). To verify homologous recombination in the mouse *Rosa26* locus, individual clones were screened by 3' genomic PCR using P1 (5'-CTCTATGGCTTCTGAGGCGGAAAG AACCAG-3') and P2 (5'-CTTTAAGAGCCATGGCAATGTTCAAGC AGG-3') primers, followed by a 5' Southern blot using EcoRI-digested DNA and a 5' external probe (Fig. 1 A). Correctly targeted ESCs were microinjected into blastocysts derived from C57BL/6 \times BDF1 mice, and chimeric male mice were crossed with C57BL/6 female mice to transmit the mutant allele to progeny. After four or five generations of backcross with C57BL/6, mice harboring the KI allele were crossed with Vav-Cre transgenic mice (de Boer et al., 2003). Recombination was confirmed by PCR with 5'-CAT CTGTAGGGCGCAGTAGTC-3' (Fig. 1 A, P3) and 5'-CCGTCGTGG TCCTGTAGTC-3' primers (Fig. 1 A, P4). We performed quantitative RT-PCR in Fig. 1 H using the following primers: N-terminal *Asxl1*, 5'-GGACTGGGGTTATGCTACCTC-3' and 5'-GCCTCGAAT GGCAGTGTG-3'; C-terminal *Asxl1*, 5'-CAGACTCTCTGTTGCTGT CC-3' and 5'-CTGTGACCTGGAGGAAGAACC-3'; and *Actb* (internal control), 5'-TGTTACCAACTGGGACGACA-3' and 5'-GGGGTG TTGAAGGTCTCAAAA-3'. The experiments were approved by the Committee on the Ethics of Animal Experiments, University of Tokyo, and all mice were maintained according to the guidelines of the Institute of Laboratory Animal Science (PA13-19, PA16-31, and PA17-26).

intergenic regions (outside -5 to 5 kb of genes). (C) Peak result of H3K4me3, *Asxl1*, and FLAG (*Asxl1* mutant) across *Id3* gene in ChIP-seq analysis. (D) Scatterplot of scores of *Asxl1* peaks and H3K4me3 (top), H2AK119Ub (middle), and H3K27me3 (bottom) peaks in WT c-Kit⁺ cells. Reads per kilobase of exon per million mapped reads (RPKM) were color coded as indicated in the bottom. The significance was determined by R^2 (the square of the Pearson correlation coefficient). (E) Scatterplot of scores of *Asxl1* peaks and the ratio of H3K4me3 peaks to H3K27me3 peaks in c-Kit⁺ control cells. RPKMs were color coded as indicated in the bottom. (F) Scatterplot of scores of FLAG peaks and the ratio of H3K4me3 peaks in c-Kit⁺ KI cells to those in c-Kit⁺ control cells. RPKMs were color coded as indicated (top). (G) Motif enrichment analysis of regions where H3K4me3 was reduced in KI c-Kit⁺ cells. Top motifs are listed.

Colony-forming assay

Primary BM cells, sorted LT-HSCs and MPPs, and Lin⁻ cells were plated in MethoCult (M3234; StemCell Technologies). MethoCult for BFU-Es (day 7), CFU-Es (day 3), CFU-GMs (day 7), and the M3434 condition (CFU-Gs, CFU-Ms, CFU-GMs, BFU-Es, CFU-GEMMs, day 10) were scored, and morphological changes of colony-forming cells were examined according to the manufacturer's protocol. Cytokine conditions were as follows: BFU-E, 50 ng/ml recombinant mouse stem cell factor (rmSCF), 10 ng/ml rmIL-3, and 4 U/ml recombinant human erythropoietin (rhEPO); CFU-E, 3 U/ml rhEPO; CFU-GM, 50 ng/ml rmSCF, 10 ng/ml rmIL-3, 10 ng/ml rmIL-6, 10 ng/ml rmGM-CSF; M3434 condition, 50 ng/ml rmSCF, 10 ng/ml rmIL-3, 10 ng/ml rhIL-6, and 3 U/ml rhEPO. All cytokines were purchased from R&D Systems.

Flow cytometry and antibodies

mAbs recognizing the following antigens were used in flow cytometry and cell sorting: CD45.2 (109813 and 109824; BioLegend), CD45.1 (110716; BioLegend), Gr-1 (108408; BioLegend), CD11b/Mac-1 (101216; BioLegend; and 12-0112-85; eBioscience), Ter-119 (116222; BioLegend; and 12-5921-83; eBioscience), CD71 (113815; BioLegend; and 553267; BD PharMingen), CD41 (133914; BioLegend), B220 (103222; BioLegend; and 12-0452-85; eBioscience), CD3 (100236; BioLegend; and 12-0031-85; eBioscience), CD117/c-Kit (105808 and 105814; BioLegend), Sca-1 (108112 and 108139; BioLegend), CD150 (115903 and 115910; BioLegend), CD48 (103427 and 103431; BioLegend), CD34 (128615; BioLegend; and 48-0341-82; eBioscience), FcγRII/III (101307 and 101327; BioLegend), human CD271/NGFR (345106; BioLegend), Ki67 (50-5698-82; eBioscience), and Annexin V (640920; BioLegend). Dead cells were eliminated by staining with DAPI (422801; BioLegend) or propidium iodide solution (421301; BioLegend). All flow cytometric analyses and cell sorting were performed on a FACSAria or FACSCalibur (BD Biosciences), and all flow cytometry data were analyzed with FlowJo software.

Purification of hematopoietic cells

Hematopoietic cells were harvested from long bones that were triturated and passed through 40-μm nylon mesh to obtain a single-cell suspension. Isolation of lineage-depleted (Lin⁻) BM cells was performed with a Lineage Cell Depletion kit (130-090-858; Miltenyi Biotec) according to the manufacturer's protocol. BM cells were incubated with a cocktail of biotinylated monoclonal antibodies against a panel of lineage antigens (CD5, B220, CD11b, Gr1, 7/4, and Ter119) and anti-Biotin MicroBeads and separated on a MACS Column in the magnetic field of a MACS Separator (Miltenyi Biotec). Lin⁻ cells were further stained with a cocktail of biotinylated lineage-specific antibodies. Then, Brilliant violet 605-conjugated streptavidin (405229; BioLegend) and a combination of mAbs, including PE-Dazzle 594- or eFluor450-conjugated anti-CD34, allophycocyanin (APC) or Brilliant violet 785 Sca-1, PE or APC-Cy7-FcγR, PE-Cy7-c-Kit, PE or APC-CD150, and APC-Cy7 or Brilliant violet 421 CD48, APC or APC-Cy7-CD45.2 mAb were used as an additional marker for donor-derived cells in the BM of B6-CD45.1 recipient mice. LSK, LT-HSC (LSK CD150⁺CD48⁻), short-term HSC (LSK CD150⁻CD48⁻), MPP (LSK CD150⁻CD48⁺), CMP (Lin⁻c-Kit⁺Sca-1⁻FcγR⁻CD34⁺), GMP

(Lin⁻c-Kit⁺Sca-1⁻FcγR⁺CD34⁺), and MEP (Lin⁻c-Kit⁺Sca-1⁻FcγR⁻CD34⁻) fractions were defined as previously described (Mayle et al., 2013). eFluor660-Ki67, APC-Annexin V, and DAPI were used as additional markers for cell cycle/apoptosis analysis as previously described (Cai et al., 2016). MkPs (CD41^{high}CD71^{low}MEP) and ErPs (CD41^{low}CD71^{high}MEP) were defined as previously described (Murphy et al., 2013).

Western blotting

Cell lysates were subjected to immunoblotting using the following antibodies: FLAG (F1804; Sigma-Aldrich), anti-Asxl1 (sc-85283; Santa Cruz Biotechnology), tubulin (B-5-1-2; Santa Cruz Biotechnology), actin (A5541; Sigma-Aldrich), and H2AK119Ub (D27C4; Cell Signaling Technology). H3K4me3 (CMA304), H3K27me3 (CMA323), and H3 were obtained from H. Kimura (Tokyo Institute of Technology, Tokyo, Japan; Kimura et al., 2008).

MOL4070A infection and inverse PCR

Newborn mice were inoculated intraperitoneally with a MOL4070LTR (MOL4070A) retrovirus solution containing ~1 × 10⁵ virus particles, which was provided by L. Wolff (National Cancer Institute, Bethesda, MD), as previously described (Wolff et al., 2003; Ikeda et al., 2016; Ueda et al., 2016). Retroviral integration sites were identified using inverse PCR as previously described (Yamasaki et al., 2010).

Sanger sequencing

PCR was performed to amplify cDNA derived from the BM cells of Vav-cre-positive *Asxl1*-MT^{fl/fl} mice using one forward (5'-TTT CACGTATCAAACCACCCTG-3') and two reverse primes (5'-AGT AGTTGTGTTCGCTGTAGATC-3' and 5'-GGTACCCTCGAGGAAGTT CC-3'). Sequencing primer (5'-ATCGTCCCGATCACGGAGTC-3') was used for the Sanger sequencing.

Transfection and retrovirus production

Retroviral production of *RUNX1*-S291fsX was performed as described previously (Watanabe-Okochi et al., 2008). *Id3* cDNA was provided by T. Ikawa (RIKEN, Yokohama, Japan). In brief, retroviruses were generated by transient transfection of *RUNX1*-S291fsX, *MLL-AF9*, *ASXL1*, or *Id3* cDNA into Plat-E packaging cells using the calcium phosphate coprecipitation method. Primary BM cells were infected with retroviruses as previously described (Watanabe-Okochi et al., 2008; Inoue et al., 2013).

Mouse BM transplantation assays

Freshly dissected femora and tibiae were isolated from Vav-Cre, Vav-Cre-negative *Asxl1*-MT^{fl/wt}, Vav-Cre-positive *Asxl1*-MT^{fl/wt}, Vav-Cre-negative *Asxl1*-MT^{fl/fl}, Vav-Cre-positive *Asxl1*-MT^{fl/fl}, and CD45.1 WT mice. BM was flushed with a 3-cc insulin syringe into cold PBS (without Ca²⁺ and Mg²⁺) supplemented with 2% BSA to generate single-cell suspensions. BM cells were spun at 1,500 rpm for 5 min by centrifugation, and RBCs were lysed in ammonium-chloride-potassium bicarbonate lysis (ACK) buffer for 5 min on ice. After centrifugation, cells were resuspended in PBS/2% BSA filtered through a 40-μm cell strainer. For competitive transplantation experiments in Fig. 4 A, 0.5 × 10⁶ total BM cells from Vav-Cre or Vav-Cre-positive *Asxl1*-MT^{fl/fl}

(CD45.2 positive) mice were mixed with WT control (CD45.1 positive) mice and transplanted via tail vein injection into 6-wk-old lethally irradiated (2×4.75 Gy) CD45.1⁺ recipient mice. Similarly, for another competitive assay (Fig. S2 C), we mixed BM cells from Vav-Cre-positive *Asx1l*-MT^{fl/wt} (GFP positive) and Vav-Cre-negative *Asx1l*-MT^{fl/wt} (GFP negative) mice and transplanted the cells into CD45.1 WT recipient mice. PB chimerism was assessed by flow cytometry. For noncompetitive transplantation experiments, 10^6 total BM cells from Vav-Cre-negative *Asx1l*-MT^{fl/wt} control (CD45.2⁺) and Vav-Cre-positive *Asx1l*-MT^{fl/wt} mice (CD45.2⁺) were injected into lethally irradiated (2×4.75 Gy) CD45.1⁺ recipient mice.

For *RUNX1*-S291fsX retroviral primary BM transplantation experiments, donor cells from Vav-Cre-negative *Asx1l*-MT^{fl/WT}, Vav-Cre-positive *Asx1l*-MT^{fl/WT}, Vav-Cre-negative *Asx1l*-MT^{fl/fl}, and Vav-Cre-positive *Asx1l*-MT^{fl/fl} mice were treated with a single dose of 150 mg/kg 5-fluoruracil followed by BM harvest from the femora and tibiae 3 d later. RBCs were removed using ACK lysis buffer, and nucleated BM cells were transduced with viral supernatants containing *RUNX1*-S291fsX for 2 d followed by tail vein injection into sublethally irradiated CD45.1 recipient mice.

Transcriptome analysis

Library preparation for whole-transcriptome analysis was performed according to the manufacturer's instructions (SureSelect Strand Specific RNA Preparation kit; Agilent Technologies). In brief, poly(A) RNA purified from 2 μ g total RNA was chemically fragmented to appropriate sizes. First-strand cDNA was synthesized from the fragmented poly(A)-selected mRNA, followed by the synthesis of second-strand cDNA. Then, adapter oligo-DNA was ligated to both ends of the double-stranded cDNA. Libraries were prepared with 12 cycles of PCR amplification of adapter-ligated cDNA using primers that are complementary to the adapters. The libraries were sequenced using a GAIIX next-generation sequencer (Illumina) using the single-end 36-bp sequencing protocol. The generated sequence tags were mapped onto the mouse genomic sequence (mm10; UCSC Genome Browser) and mRNA expression levels were normalized as reads per kilobase per million. We validated RNA-sequencing data by quantitative RT-PCR using the following primers: *Id3*, 5'-CTGTCGGAACGTAGCCTGG-3' and 5'-GTGGTTCATGTCGTCCAAGAG-3'; *Gata1*, 5'-TATGGC AAGACGGCACTCTAC-3' and 5'-GGTGTCCAAGAAGCTGTTGTT-3'; *Runx1*, 5'-GATGGCACTCTGGTCACCG-3' and 5'-GCCGCTCGG AAAAGGACAA-3'; *Sox6*, 5'-ACCAGTGACTTCTGGGTGCT-3' and 5'-CAAGTCCTGGGTCAATTGCTT-3'; *Tjp1*, 5'-GCTTTAGCGAACAGA AGGAGC-3' and 5'-TTCATTTTCCGAGACTTCACCA-3'; *Hba-a1*, 5'-CACCACCAAGACCTACTTCCC-3' and 5'-CAGTGGCTCAGGAGC TTGA-3'; and *Actb*, 5'-TGTTACCAACTGGGACGACA-3' and 5'-GGG GTGTTGAAGGTCTCAAA-3'.

ChIP-seq

For ChIP-seq in mouse cells, 10 million BM c-Kit⁺ cells isolated with anti-mouse c-Kit Biotin (13–1171-85; eBioscience) and anti-Biotin Microbeads (130–090-485; Miltenyi Biotec) were used. In brief, cells were fixed in a 1% methanol-free formaldehyde solution and then resuspended in SDS lysis buffer. Lysates were sonicated in an E220 focused ultrasonicator (Covaris) to a desired

fragment size distribution of 100–500 bp. Immunoprecipitation reactions were performed with the following antibodies, each on ~500,000 cells as previously described (Krivtsov et al., 2008). Antibodies used for ChIP include anti-H3K4me3 (9751S; Cell Signaling), anti-H3K27me3 (07-449; Millipore), anti-H2AK119Ub (8240; Cell Signaling), anti-Asx1l (sc-85283; Santa Cruz Biotechnology), and anti-FLAG (F1804; Sigma-Aldrich). ChIP assays were processed and barcoded library and raw data analyses were performed as previously described (Micol et al., 2017).

Statistical analyses

Statistical significance was determined by unpaired Student's *t* test or ANOVA after testing for normal distribution and equal variance, unless indicated otherwise. For Kaplan–Meier survival analysis, the Mantel–Cox log-rank test was used to determine statistical significance. Data were plotted using GraphPad Prism 8 software as mean values; error bars represent SD.

Accession numbers for RNA-seq and ChIP-seq

RNA-sequencing and ChIP-seq data have been deposited into the NCBI Gene Expression Omnibus portal under the accession no. GSE111067.

Online supplemental material

Fig. S1 shows additional characterization of *Asx1l*-MT KI mice. Fig. S2 shows additional characterization of HSC and progenitor cells of KI mice. Fig. S3 shows transcriptional and epigenetic effects in KI mice. Fig. S4 shows the effects of *Asx1l* mutant expression on histone modification. Table S1 contains the motif enrichment analysis of *Asx1l* mutant and *Asx1l*-WT binding sites.

Acknowledgments

We acknowledge Dr. Linda Wolff, Dr. Yoshiteru Sasaki, Dr. Haruhiko Koseki, Dr. Tomokatsu Ikawa, and Dr. Hiroshi Kimura for providing materials described above.

D. Inoue is supported by the Friends of Leukemia Research Fund and the Japan Society for the Promotion of Science KAKENHI Grant-in-Aid for Young Scientists (26893051) and Overseas Research Fellowships. D. Inoue and O. Abdel-Wahab are supported by the Leukemia and Lymphoma Society. T. Kitamura is supported by the Japan Society for the Promotion of Science KAKENHI Grant-in-Aid for Scientific Research (B 15H04855), a research grant from the Tokyo Biochemical Research Foundation, and a research grant from the Uehara Memorial Foundation. O. Abdel-Wahab is supported by the US Department of Defense Bone Marrow Failure Research Program (grant W81XWH-12-1-0041), the Edward P. Evans Foundation, the Taub Foundation, and the Starr Foundation (grants I8-A8-075 and I9-A9-059).

The authors declare no competing financial interests.

Author contributions: D. Inoue, R. Nagase, H. Honda, T. Fujino, O. Abdel-Wahab, and T. Kitamura designed the study. R. Nagase, D. Inoue, T. Fujino, A. Pastore, N. Yamasaki, H. Honda, H.-A. Hou, Y. Sera, and H.-F. Tien performed experiments and analyzed data. R. Nagase, D. Inoue, A. Pastore, and A. Kanai performed RNA-seq and ChIP-seq analyses. D. Inoue, R. Nagase, O. Abdel-Wahab, and T. Kitamura prepared the manuscript with help from all coauthors.

Submitted: 27 June 2017
 Revised: 24 December 2017
 Accepted: 1 March 2018

References

- Abdel-Wahab, O., M. Adli, L.M. LaFave, J. Gao, T. Hricik, A.H. Shih, S. Pandey, J.P. Patel, Y.R. Chung, R. Koche, et al. 2012. ASXL1 mutations promote myeloid transformation through loss of PRC2-mediated gene repression. *Cancer Cell*. 22:180–193. <https://doi.org/10.1016/j.ccr.2012.06.032>
- Abdel-Wahab, O., J. Gao, M. Adli, A. Dey, T. Trimarchi, Y.R. Chung, C. Kusc, T. Hricik, D. Ndiaye-Lobry, L.M. Lafave, et al. 2013. Deletion of Asxl1 results in myelodysplasia and severe developmental defects in vivo. *J. Exp. Med.* 210:2641–2659. <https://doi.org/10.1084/jem.20131141>
- Addya, S., M.A. Keller, K. Delgrosso, C.M. Ponte, R. Vadigepalli, G.E. Gonye, and S. Surrey. 2004. Erythroid-induced commitment of K562 cells results in clusters of differentially expressed genes enriched for specific transcription regulatory elements. *Physiol. Genomics*. 19:117–130. <https://doi.org/10.1152/physiolgenomics.00028.2004>
- Balasubramani, A., A. Larjo, J.A. Bassein, X. Chang, R.B. Hastie, S.M. Togher, H. Lähdesmäki, and A. Rao. 2015. Cancer-associated ASXL1 mutations may act as gain-of-function mutations of the ASXL1-BAP1 complex. *Nat. Commun.* 6:7307. <https://doi.org/10.1038/ncomms8307>
- Behrens, K., K. Maul, N. Tekin, N. Kriebitzsch, D. Indenbirken, V. Prassolov, U. Müller, H. Serve, J. Cammenga, and C. Stöcking. 2017. RUNX1 cooperates with FLT3-ITD to induce leukemia. *J. Exp. Med.* 214:737–752.
- Bejar, R., K. Stevenson, O. Abdel-Wahab, N. Galili, B. Nilsson, G. Garcia-Manero, H. Kantarjian, A. Raza, R.L. Levine, D. Neuberg, and B.L. Ebert. 2011. Clinical effect of point mutations in myelodysplastic syndromes. *N. Engl. J. Med.* 364:2496–2506. <https://doi.org/10.1056/NEJMoa1013343>
- Blank, U., and S. Karlsson. 2015. TGF- β signaling in the control of hematopoietic stem cells. *Blood*. 125:3542–3550. <https://doi.org/10.1182/blood-2014-12-618090>
- Cai, Q., R. Jeannot, W.K. Hua, G.J. Cook, B. Zhang, J. Qi, H. Liu, L. Li, C.C. Chen, G. Marcucci, and Y.H. Kuo. 2016. CBF β -SMMHC creates aberrant megakaryocyte-erythroid progenitors prone to leukemia initiation in mice. *Blood*. 128:1503–1515. <https://doi.org/10.1182/blood-2016-01-693119>
- Cantù, C., R. Ierardi, I. Alborelli, C. Fugazza, L. Cassinelli, S. Piconese, F. Bosè, S. Ottolenghi, G. Ferrari, and A. Ronchi. 2011. Sox6 enhances erythroid differentiation in human erythroid progenitors. *Blood*. 117:3669–3679. <https://doi.org/10.1182/blood-2010-04-282350>
- Chen, K., J. Liu, S. Heck, J.A. Chasis, X. An, and N. Mohandas. 2009. Resolving the distinct stages in erythroid differentiation based on dynamic changes in membrane protein expression during erythropoiesis. *Proc. Natl. Acad. Sci. USA*. 106:17413–17418. <https://doi.org/10.1073/pnas.0909296106>
- Chen, T.C., H.A. Hou, W.C. Chou, J.L. Tang, Y.Y. Kuo, C.Y. Chen, M.H. Tseng, C.F. Huang, Y.J. Lai, Y.C. Chiang, et al. 2014. Dynamics of ASXL1 mutation and other associated genetic alterations during disease progression in patients with primary myelodysplastic syndrome. *Blood Cancer J.* 4:e177. <https://doi.org/10.1038/bcj.2013.74>
- Cook, G.J., and T.S. Pardee. 2013. Animal models of leukemia: any closer to the real thing? *Cancer Metastasis Rev.* 32:63–76. <https://doi.org/10.1007/s10555-012-9405-5>
- de Boer, J., A. Williams, G. Skavdis, N. Harker, M. Coles, M. Tolaini, T. Norton, K. Williams, K. Roderick, A.J. Potocnik, and D. Kioussis. 2003. Transgenic mice with hematopoietic and lymphoid specific expression of Cre. *Eur. J. Immunol.* 33:314–325. <https://doi.org/10.1002/immu.200310005>
- Deed, R.W., M. Jasiok, and J.D. Norton. 1998. Lymphoid-specific expression of the Id3 gene in hematopoietic cells. Selective antagonism of E2A basic helix-loop-helix protein associated with Id3-induced differentiation of erythroleukemia cells. *J. Biol. Chem.* 273:8278–8286. <https://doi.org/10.1074/jbc.273.14.8278>
- Deplus, R., B. Delatte, M.K. Schwinn, M. Defrance, J. Méndez, N. Murphy, M.A. Dawson, M. Volkmar, P. Putmans, E. Calonne, et al. 2013. TET2 and TET3 regulate GlcNAcylation and H3K4 methylation through OGT and SET1/COMPASS. *EMBO J.* 32:645–655. <https://doi.org/10.1038/emboj.2012.357>
- Dey, A., D. Seshasayee, R. Noubade, D.M. French, J. Liu, M.S. Chaurushiya, D.S. Kirkpatrick, V.C. Pham, J.R. Lill, C.E. Bakalarski, et al. 2012. Loss of the tumor suppressor BAP1 causes myeloid transformation. *Science*. 337:1541–1546. <https://doi.org/10.1126/science.1221711>
- Döhner, H., E. Estey, D. Grimwade, S. Amadori, F.R. Appelbaum, T. Büchner, H. Dombret, B.L. Ebert, P. Fenau, R.A. Larson, et al. 2017. Diagnosis and management of AML in adults: 2017 ELN recommendations from an international expert panel. *Blood*. 129:424–447. <https://doi.org/10.1182/blood-2016-08-733196>
- Genovese, G., A.K. Kähler, R.E. Handsaker, J. Lindberg, S.A. Rose, S.F. Bakhoum, K. Chambert, E. Mick, B.M. Neale, M. Fromer, et al. 2014. Clonal hematopoiesis and blood-cancer risk inferred from blood DNA sequence. *N. Engl. J. Med.* 371:2477–2487. <https://doi.org/10.1056/NEJMoa1409405>
- Goyama, S., J. Schibler, L. Cunningham, Y. Zhang, Y. Rao, N. Nishimoto, M. Nakagawa, A. Olsson, M. Wunderlich, K.A. Link, et al. 2013. Transcription factor RUNX1 promotes survival of acute myeloid leukemia cells. *J. Clin. Invest.* 123:3876–3888. <https://doi.org/10.1172/JCI68557>
- Haferlach, T., Y. Nagata, V. Grossmann, Y. Okuno, U. Bacher, G. Nagae, S. Schnittger, M. Sanada, A. Kon, T. Alpermann, et al. 2014. Landscape of genetic lesions in 944 patients with myelodysplastic syndromes. *Leukemia*. 28:241–247. <https://doi.org/10.1038/leu.2013.336>
- Harada, Y., and H. Harada. 2009. Molecular pathways mediating MDS/AML with focus on AML1/RUNX1 point mutations. *J. Cell. Physiol.* 220:16–20. <https://doi.org/10.1002/jcp.21769>
- Hess, J.L., C.B. Bittner, D.T. Zeisig, C. Bach, U. Fuchs, A. Borkhardt, J. Frampton, and R.K. Slany. 2006. c-Myb is an essential downstream target for homeobox-mediated transformation of hematopoietic cells. *Blood*. 108:297–304. <https://doi.org/10.1182/blood-2005-12-5014>
- Ikeda, K., T. Ueda, N. Yamasaki, Y. Nakata, Y. Sera, A. Nagamachi, T. Miyama, H. Kobayashi, K. Takubo, A. Kanai, et al. 2016. Maintenance of the functional integrity of mouse hematopoiesis by EED and promotion of leukemogenesis by EED haploinsufficiency. *Sci. Rep.* 6:29454. <https://doi.org/10.1038/srep29454>
- Inoue, D., J. Kitaura, K. Togami, K. Nishimura, Y. Enomoto, T. Uchida, Y. Kagiya, K.C. Kawabata, F. Nakahara, K. Izawa, et al. 2013. Myelodysplastic syndromes are induced by histone methylation-altering ASXL1 mutations. *J. Clin. Invest.* 123:4627–4640. <https://doi.org/10.1172/JCI70739>
- Inoue, D., J. Kitaura, H. Matsui, H.A. Hou, W.C. Chou, A. Nagamachi, K.C. Kawabata, K. Togami, R. Nagase, S. Horikawa, et al. 2015. SETBP1 mutations drive leukemic transformation in ASXL1-mutated MDS. *Leukemia*. 29:847–857. <https://doi.org/10.1038/leu.2014.301>
- Inoue, D., M. Matsumoto, R. Nagase, M. Saika, T. Fujino, K.I. Nakayama, and T. Kitamura. 2016. Truncation mutants of ASXL1 observed in myeloid malignancies are expressed at detectable protein levels. *Exp. Hematol.* 44:172–176.
- Inoue, D., T. Fujino, P. Sheridan, Y.Z. Zhang, R. Nagase, S. Horikawa, Z. Li, H. Matsui, A. Kanai, M. Saika, et al. 2018. A novel ASXL1-OGT axis plays roles in H3K4 methylation and tumor suppression in myeloid malignancies. *Leukemia*. <https://doi.org/10.1038/s41375-018-0083-3>
- Jaiswal, S., P. Fontanillas, J. Flannick, A. Manning, P.V. Grauman, B.G. Mar, R.C. Lindsley, C.H. Mermel, N. Burt, A. Chavez, et al. 2014. Age-related clonal hematopoiesis associated with adverse outcomes. *N. Engl. J. Med.* 371:2488–2498. <https://doi.org/10.1056/NEJMoa1408617>
- Kamminga, L.M., L.V. Bystrykh, A. de Boer, S. Houwer, J. Douma, E. Weersing, B. Döntje, and G. de Haan. 2006. The Polycomb group gene *Ezh2* prevents hematopoietic stem cell exhaustion. *Blood*. 107:2170–2179. <https://doi.org/10.1182/blood-2005-09-3585>
- Kimura, H., Y. Hayashi-Takanaka, Y. Goto, N. Takizawa, and N. Nozaki. 2008. The organization of histone H3 modifications as revealed by a panel of specific monoclonal antibodies. *Cell Struct. Funct.* 33:61–73. <https://doi.org/10.1247/csf.07035>
- Krivtsov, A.V., Z. Feng, M.E. Lemieux, J. Faber, S. Vempati, A.U. Sinha, X. Xia, J. Jesneck, A.P. Bracken, L.B. Silverman, et al. 2008. H3K79 methylation profiles define murine and human MLL-AF4 leukemias. *Cancer Cell*. 14:355–368. <https://doi.org/10.1016/j.ccr.2008.10.001>
- Liu, J., J. Zhang, Y. Ginzburg, H. Li, F. Xue, L. De Franceschi, J.A. Chasis, N. Mohandas, and X. An. 2013. Quantitative analysis of murine terminal erythroid differentiation in vivo: novel method to study normal and disordered erythropoiesis. *Blood*. 121:e43–e49. <https://doi.org/10.1182/blood-2012-09-456079>
- Mayle, A., M. Luo, M. Jeong, and M.A. Goodell. 2013. Flow cytometry analysis of murine hematopoietic stem cells. *Cytometry A*. 83:27–37. <https://doi.org/10.1002/cyto.a.22093>
- Micol, J.B., A. Pastore, D. Inoue, N. Duployez, E. Kim, S.C. Lee, B.H. Durham, Y.R. Chung, H. Cho, X.J. Zhang, et al. 2017. ASXL2 is essential for haematopoiesis and acts as a haploinsufficient tumour suppressor in leukemia. *Nat. Commun.* 8:15429. <https://doi.org/10.1038/ncomms15429>
- Milne, T.A., D.A. Sinclair, and H.W. Brock. 1999. The Additional sex combs gene of *Drosophila* is required for activation and repression of homeotic loci, and interacts specifically with Polycomb and super sex combs. *Mol. Gen. Genet.* 261:753–761. <https://doi.org/10.1007/s004380050018>

- Murphy, A.J., N. Bijl, L. Yvan-Charvet, C.B. Welch, N. Bhagwat, A. Rehemian, Y. Wang, J.A. Shaw, R.L. Levine, H. Ni, et al. 2013. Cholesterol efflux in megakaryocyte progenitors suppresses platelet production and thrombocytosis. *Nat. Med.* 19:586–594. <https://doi.org/10.1038/nm.3150>
- Ng, S.Y., T. Yoshida, J. Zhang, and K. Georgopoulos. 2009. Genome-wide lineage-specific transcriptional networks underscore Ikaros-dependent lymphoid priming in hematopoietic stem cells. *Immunity*. 30:493–507. <https://doi.org/10.1016/j.immuni.2009.01.014>
- Papaemmanuil, E., M. Gerstung, L. Mälvqvist, S. Tauro, G. Gundem, P. Van Loo, C.J. Yoon, P. Ellis, D.C. Wedge, A. Pellagatti, et al. Chronic Myeloid Disorders Working Group of the International Cancer Genome Consortium. 2013. Clinical and biological implications of driver mutations in myelodysplastic syndromes. *Blood*. 122:3616–3627, quiz:3699. <https://doi.org/10.1182/blood-2013-08-518886>
- Paschka, P., R.F. Schlenk, V.I. Gaidzik, J.K. Herzig, T. Aulitzky, L. Bullinger, D. Späth, V. Teleanu, A. Kündgen, C.H. Köhne, et al. 2015. ASXL1 mutations in younger adult patients with acute myeloid leukemia: a study by the German-Austrian Acute Myeloid Leukemia Study Group. *Haematologica*. 100:324–330. <https://doi.org/10.3324/haematol.2014.114157>
- Paulson, R.F. 2014. Targeting a new regulator of erythropoiesis to alleviate anemia. *Nat. Med.* 20:334–335. <https://doi.org/10.1038/nm.3524>
- Pietras, E.M., D. Reynaud, Y.A. Kang, D. Carlin, F.J. Calero-Nieto, A.D. Leavitt, J.M. Stuart, B. Göttgens, and E. Passequé. 2015. Functionally Distinct Subsets of Lineage-Biased Multipotent Progenitors Control Blood Production in Normal and Regenerative Conditions. *Cell Stem Cell*. 17:35–46. <https://doi.org/10.1016/j.stem.2015.05.003>
- Quesada, V., L. Conde, N. Villamor, G.R. Ordóñez, P. Jares, L. Bassaganyas, A.J. Ramsay, S. Beà, M. Pinyol, A. Martínez-Trillos, et al. 2011. Exome sequencing identifies recurrent mutations of the splicing factor SF3B1 gene in chronic lymphocytic leukemia. *Nat. Genet.* 44:47–52. <https://doi.org/10.1038/ng.1032>
- Riz, I., S.S. Akimov, S.S. Eaker, K.K. Baxter, H.J. Lee, L. Mariño-Ramírez, D. Landsman, T.S. Hawley, and R.G. Hawley. 2007. TLX1/HOX11-induced hematopoietic differentiation blockade. *Oncogene*. 26:4115–4123. <https://doi.org/10.1038/sj.onc.1210185>
- Sanchez-Pulido, L., L. Kong, and C.P. Ponting. 2012. A common ancestry for BAP1 and Uch37 regulators. *Bioinformatics*. 28:1953–1956. <https://doi.org/10.1093/bioinformatics/bts319>
- Scheuermann, J.C., A.G. de Ayala Alonso, K. Oktaba, N. Ly-Hartig, R.K. McGinty, S. Fraterman, M. Wilm, T.W. Muir, and J. Müller. 2010. Histone H2A deubiquitinase activity of the Polycomb repressive complex PR-DUB. *Nature*. 465:243–247. <https://doi.org/10.1038/nature08966>
- Schuhmacher, M., F. Kohlhuber, M. Hölzel, C. Kaiser, H. Burtscher, M. Jarsch, G.W. Bornkamm, G. Laux, A. Polack, U.H. Weidle, and D. Eick. 2001. The transcriptional program of a human B cell line in response to Myc. *Nucleic Acids Res.* 29:397–406. <https://doi.org/10.1093/nar/29.2.397>
- Shi, H., S. Yamamoto, M. Sheng, J. Bai, P. Zhang, R. Chen, S. Chen, L. Shi, O. Abdel-Wahab, M. Xu, et al. 2016. ASXL1 plays an important role in erythropoiesis. *Sci. Rep.* 6:28789. <https://doi.org/10.1038/srep28789>
- Shields, B.J., J.T. Jackson, D. Metcalf, W. Shi, Q. Huang, A.L. Garnham, S.P. Glaser, D. Beck, J.E. Pimanda, C.W. Bogue, et al. 2016. Acute myeloid leukemia requires Hhex to enable PRC2-mediated epigenetic repression of Cdkn2a. *Genes Dev.* 30:78–91. <https://doi.org/10.1101/gad.268425.115>
- Sowa, M.E., E.J. Bennett, S.P. Gygi, and J.W. Harper. 2009. Defining the human deubiquitinating enzyme interaction landscape. *Cell*. 138:389–403. <https://doi.org/10.1016/j.cell.2009.04.042>
- Suzuki, M., T. Moriguchi, K. Ohneda, and M. Yamamoto. 2009. Differential contribution of the Gata1 gene hematopoietic enhancer to erythroid differentiation. *Mol. Cell. Biol.* 29:1163–1175. <https://doi.org/10.1128/MCB.01572-08>
- Suzuki, M., M. Kobayashi-Osaki, S. Tsutsumi, X. Pan, S. Ohmori, J. Takai, T. Moriguchi, O. Ohneda, K. Ohneda, R. Shimizu, et al. 2013. GATA factor switching from GATA2 to GATA1 contributes to erythroid differentiation. *Genes Cells*. 18:921–933.
- Thol, F., I. Friesen, F. Damm, H. Yun, E.M. Weissinger, J. Krauter, K. Wagner, A. Chaturvedi, A. Sharma, M. Wichmann, et al. 2011. Prognostic significance of ASXL1 mutations in patients with myelodysplastic syndromes. *J. Clin. Oncol.* 29:2499–2506. <https://doi.org/10.1200/JCO.2010.33.4938>
- Tyagi, S., A.L. Chabes, J. Wysocka, and W. Herr. 2007. E2F activation of S phase promoters via association with HCF-1 and the MLL family of histone H3K4 methyltransferases. *Mol. Cell*. 27:107–119. <https://doi.org/10.1016/j.molcel.2007.05.030>
- Ueda, T., Y. Nakata, A. Nagamachi, N. Yamasaki, A. Kanai, Y. Sera, M. Sasaki, H. Matsui, Z. Honda, H. Oda, et al. 2016. Propagation of trimethylated H3K27 regulated by polycomb protein EED is required for embryogenesis, hematopoietic maintenance, and tumor suppression. *Proc. Natl. Acad. Sci. USA*. 113:10370–10375. <https://doi.org/10.1073/pnas.1600070113>
- Vardiman, J.W., J. Thiele, D.A. Arber, R.D. Brunning, M.J. Borowitz, A. Porwit, N.L. Harris, M.M. Le Beau, E. Hellström-Lindberg, A. Tefferi, and C.D. Bloomfield. 2009. The 2008 revision of the World Health Organization (WHO) classification of myeloid neoplasms and acute leukemia: rationale and important changes. *Blood*. 114:937–951. <https://doi.org/10.1182/blood-2009-03-209262>
- Wang, J., Z. Li, Y. He, F. Pan, S. Chen, S. Rhodes, L. Nguyen, J. Yuan, L. Jiang, X. Yang, et al. 2014. Loss of Asxl1 leads to myelodysplastic syndrome-like disease in mice. *Blood*. 123:541–553. <https://doi.org/10.1182/blood-2013-05-500272>
- Watanabe-Okochi, N., J. Kitaura, R. Ono, H. Harada, Y. Harada, Y. Komeno, H. Nakajima, T. Nosaka, T. Inaba, and T. Kitamura. 2008. AML1 mutations induced MDS and MDS/AML in a mouse BMT model. *Blood*. 111:4297–4308. <https://doi.org/10.1182/blood-2007-01-068346>
- Will, B., T.O. Vogler, S. Narayanagari, B. Bartholdy, T.I. Todorova, M. da Silva Ferreira, J. Chen, Y. Yu, J. Mayer, L. Barreyro, et al. 2015. Minimal PU.1 reduction induces a preleukemic state and promotes development of acute myeloid leukemia. *Nat. Med.* 21:1172–1181. <https://doi.org/10.1038/nm.3936>
- Wolff, L., R. Koller, X. Hu, and M.R. Anver. 2003. A Moloney murine leukemia virus-based retrovirus with 4070A long terminal repeat sequences induces a high incidence of myeloid as well as lymphoid neoplasms. *J. Virol.* 77:4965–4971. <https://doi.org/10.1128/JVI.77.8.4965-4971.2003>
- Xie, M., C. Lu, J. Wang, M.D. McLellan, K.J. Johnson, M.C. Wendl, J.F. McMichael, H.K. Schmidt, V. Yellapantula, C.A. Miller, et al. 2014. Age-related mutations associated with clonal hematopoietic expansion and malignancies. *Nat. Med.* 20:1472–1478. <https://doi.org/10.1038/nm.3733>
- Yamasaki, N., K. Miyazaki, A. Nagamachi, R. Koller, H. Oda, M. Miyazaki, T. Sasaki, Z.I. Honda, L. Wolff, T. Inaba, and H. Honda. 2010. Identification of Zfp521/ZNF521 as a cooperative gene for E2A-HLF to develop acute B-lineage leukemia. *Oncogene*. 29:1963–1975.
- Yokomizo, T., K. Hasegawa, H. Ishitobi, M. Osato, M. Ema, Y. Ito, M. Yamamoto, and S. Takahashi. 2008. Runx1 is involved in primitive erythropoiesis in the mouse. *Blood*. 111:4075–4080. <https://doi.org/10.1182/blood-2007-05-091637>
- Yokoyama, A., Z. Wang, J. Wysocka, M. Sanyal, D.J. Aulifero, I. Kitabayashi, W. Herr, and M.L. Cleary. 2004. Leukemia proto-oncoprotein MLL forms a SET1-like histone methyltransferase complex with menin to regulate Hox gene expression. *Mol. Cell. Biol.* 24:5639–5649. <https://doi.org/10.1128/MCB.24.13.5639-5649.2004>
- Zhang, J., L. Ding, L. Holmfeldt, G. Wu, S.L. Heatley, D. Payne-Turner, J. Easton, X. Chen, J. Wang, M. Rusch, et al. 2012. The genetic basis of early T-cell precursor acute lymphoblastic leukaemia. *Nature*. 481:157–163. <https://doi.org/10.1038/nature10725>
- Zhao, Q., C. Chang, J.P. Gonzalez, K. Alzahrani, J.L. Button, and D. Fraidenraich. 2016. Combined Id1 and Id3 Deletion Leads to Severe Erythropoietic Disturbances. *PLoS One*. 11:e0154480. <https://doi.org/10.1371/journal.pone.0154480>
- Zhou, P., Z. Wang, X. Yuan, C. Zhou, L. Liu, X. Wan, F. Zhang, X. Ding, C. Wang, S. Xiong, et al. 2013. Mixed lineage leukemia 5 (MLL5) protein regulates cell cycle progression and E2F1-responsive gene expression via association with host cell factor-1 (HCF-1). *J. Biol. Chem.* 288:17532–17543. <https://doi.org/10.1074/jbc.M112.439729>